Assessing drug safety by identifying the axis of arrhythmia in cardiomyocyte electrophysiology

Stewart Heitmann [1,✉], **Jamie I Vandenberg** [1,2], **and Adam P Hill** [1,2,3]

[1]Victor Chang Cardiac Research Institute, Darlinghurst, NSW 2010, Australia; [2]School of Clinical Medicine, Faculty of Medicine and Health, UNSW Sydney, Australia; [3]Victor Chang Cardiac Research Institute Innovation Centre, Darlinghurst, NSW 2010, Australia

Many classes of drugs can induce fatal cardiac arrhythmias by disrupting the electrophysiology of cardiomyocytes. Safety guidelines thus require all new drugs to be assessed for pro-arrhythmic risk prior to conducting human trials. The standard safety protocols primarily focus on drug blockade of the delayed-rectifier potassium current (IKr). Yet the risk is better assessed using four key ion currents (IKr, ICaL, INaL, IKs). We simulated 100,000 phenotypically diverse cardiomyocytes to identify the underlying relationship between the blockade of those currents and the emergence of ectopic beats in the action potential. We call that relationship the axis of arrhythmia. It serves as a yardstick for quantifying the arrhythmogenic risk of any drug from its profile of multi-channel block alone. We tested it on 109 drugs and found that it predicted the clinical risk labels to an accuracy of 88.1% to 90.8%. Pharmacologists can use our method to assess the safety of novel drugs without resort to animal testing nor unwieldy computer simulations.

cardiotoxicity | arrhythmia | safety pharmacology | electrophysiology

Correspondence: ***s.heitmann @victorchang.edu.au***

Introduction

Torsades des Pointes is a potentially lethal ventricular arrhythmia that can be induced by many classes of drugs. These include antibiotics, antipsychotics, antihistamines, chemotherapeutics and antiarrhythmics (Yap and Camm, 2003). The majority of torsadogenic drugs block the hERG ion channel which carries the delayed-rectifier potassium current (I_{Kr}) (Witchel, 2011). For this reason, international safety guidelines require hERG block to be assessed in living cells prior to conducting human trials (ICH Harmonised Tripartite Guideline, 2005). However, the standard hERG assay is overly sensitive. It does not accommodate multi-channel effects which render some drugs safe despite blocking hERG (Martin et al., 2004; Hoffmann and Warner, 2006). Consequently, many useful drugs are prematurely abandoned during pre-clinical trials. The safety pharmacology community are actively pursuing new *in vitro* and *in silico* assays that improve accuracy by targeting multiple ion channels (Pugsley et al., 2008; Colatsky et al., 2016).

In silico assays use computational models of cardiomyocyte electrophysiology in place of a living cell (Mirams et al., 2011; Lancaster and Sobie, 2016; Mann et al., 2016; Dutta et al., 2017; Passini et al., 2017; Ballouz et al., 2020; Llopis-Lorente et al., 2020). Drug blockade (Figure 1A) is simulated in the model (Figure 1B) by attenuating the conductivity of the relevant ion currents. The conductance parameters are labeled G by convention. The simulations can be repeated across a diverse range of cardiac phenotypes to ensure generality of the results (Britton et al., 2013; Ni et al., 2018; Gong and Sobie, 2018). The individual phenotypes are constructed by randomizing the conductance parameters to mimic natural variation in ion channel expression. The method produces a population of cardiac action potentials (Figure 1C). Selected biomarkers within the action potentials are then statistically analyzed for drug-induced changes (e.g. Hondeghem, 2005; Varshneya et al., 2021). Contemporary research is largely concerned with improving those biomarkers.

Yet the main problem with the conventional approach is that it requires multitudes of computationally intensive simulations for every drug that is assessed. Pharmacology laboratories must invest heavily in specialist computing resources and expertise before they can apply the methods to their own drugs. We propose a new approach that allows drugs to be assessed without conducting drug-specific simulations. The method is initiated by simulating a diverse population of cardiomy-

Significance Statement

Many classes of drugs interfere with the electrical signaling of the heart, leading to arrhythmias and cardiac arrest. Newly developed drugs must therefore undergo mandatory safety testing in animals prior to human trials. Computational models of cardiac electrophysiology offer an ethical alternative but the current methods are difficult to apply beyond specialist computing laboratories. This study uses such models to identify the underlying relationship between drugs and cardiac arrhythmias. Those findings are then translated into a compact metric that can be applied using simple pen and paper calculations. The new metric allows pharmacology laboratories to assess the safety of novel drugs without using animals nor unwieldy computer simulations.

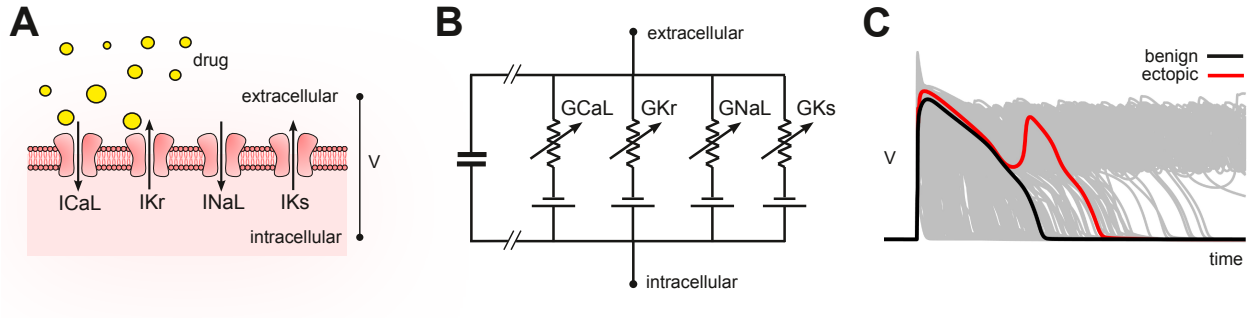

Figure 1. Conceptual framework. (**A**) Drugs simultaneously block multiple species of ion channels to differing degrees. The principal ion currents implicated in drug-induced Torsades des Pointes are $I_{\text{CaL}}, I_{\text{Kr}}, I_{\text{NaL}}$ and I_{Ks}. (**B**) Simplified circuit diagram of cardiomyocyte electrophysiology. Drug blockade is simulated by attenuating the ionic conductances $(G_{\text{CaL}}, G_{\text{Kr}}, G_{\text{NaL}}, G_{\text{Ks}})$. Those parameters are also varied randomly to mimic individual differences in electrophysiology. (**C**) Simulated action potentials of phenotypically diverse cardiomyocytes. Early after-depolarizations (red) are biomarkers for Torsades des Pointes. Conventional *in silico* assays simulate the effect of drugs on cardiomyocytes on a case by case basis. Our method inverts the procedure by simulating cardiomyocytes in the absence of drugs and then inferring how drugs would behave.

ocytes in the absence of drugs. That simulation need only be done once. The drug-free population is then used to identify the principal relationship between ionic conductances and ectopic phenotypes. We call that relationship the *axis of arrhythmia* because it describes the principal pathway for transforming benign cardiomyocytes into ecoptic cardiomyocytes. Thereafter, the axis serves as a yardstick for assessing the torsadogenic risk of drugs directly from their physiological signature of ion channel blockade alone.

Results

The action potentials of 100,000 randomized ventricular cardiomyocytes (Figure 2A) were simulated using a variant of the O'Hara-Rudy model (O'Hara et al., 2011) that was optimized for long-QT syndrome (Mann et al., 2016; Krogh-Madsen et al., 2017). Early after-depolarizations were chosen as a biomarker for Torsades des Pointes. Cardiomyocytes that exhibited them were classified as *ectopic* (red) and those that did not were classified as *benign* (gray).

The four cardiac ion currents that we investigated $(I_{\text{CaL}}, I_{\text{Kr}}, I_{\text{NaL}}, I_{\text{Ks}})$ have previously been implicated in torsadogenic risk (Dutta et al., 2017; Llopis-Lorente et al., 2020). The myocytes were constructed by re-scaling the conductance parameters $(G_{\text{CaL}}, G_{\text{Kr}}, G_{\text{NaL}}, G_{\text{Ks}})$ with randomly selected multipliers that were drawn uniformly from a logarithmic scale (Figure 2B). The use of the logarithmic coordinate frame is crucial to our subsequent analysis.

The ectopic and benign phenotypes were found to be clearly segregated in parameter space (Figures 2C and 2D). Multivariate logistic regression was used to identify the linear boundary (dashed line) that best separated the two classes. We refer to it as the *decision boundary* following the conventions of classification statistics.

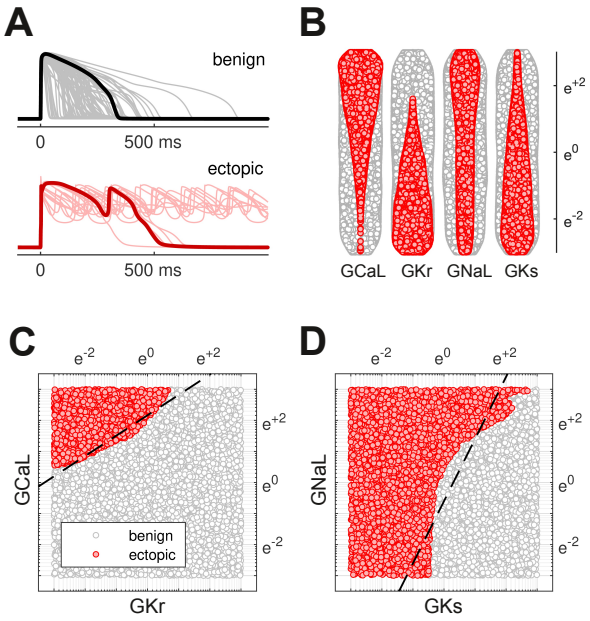

Figure 2. Benign versus ectopic cardiac phenotypes. (**A**) Simulated action potentials for cardiomyocytes with randomly scaled conductance parameters G_{Kr}, G_{CaL}, G_{NaL} and G_{Ks}. Myocytes that exhibited early after-depolarizations were classified as *ectopic* (red). Those that did not were classified as *benign* (gray). (**B**) Swarm plots of the conductance scalars on a logarithmic scale. Color indicates the classification of the myocyte (benign versus ectopic). (**C**) Two-dimensional slice of parameter space showing the relationship between ectopic and benign phenotypes in G_{CaL} versus G_{Kr}. The dashed line is the statistical decision boundary. G_{NaL} and G_{Ks} were fixed at unity $(e^0 = 1)$. (**D**) Two-dimensional slice showing G_{NaL} versus G_{Ks}. In this case G_{CaL} is $e^{0.46}$ and G_{Kr} is $e^{-2.3}$.

Decision boundary

The multivariate logistic regression equation,

$$\ln \frac{p}{1-p} = \beta_0 + \beta_{\text{CaL}} X_{\text{CaL}} + \beta_{\text{Kr}} X_{\text{Kr}} + \beta_{\text{NaL}} X_{\text{NaL}} + \beta_{\text{Ks}} X_{\text{Ks}}, \quad (1)$$

describes the log-odds of a cardiomyocyte being ectopic where $X_{\text{CaL}} = \ln(G_{\text{CaL}})$, $X_{\text{Kr}} = \ln(G_{\text{Kr}})$, $X_{\text{NaL}} = \ln(G_{\text{NaL}})$ and $X_{\text{Ks}} = \ln(G_{\text{Ks}})$. The decision boundary is the hyperplane in four-dimensional parameter space $(X_{\text{CaL}}, X_{\text{Kr}}, X_{\text{NaL}}, X_{\text{Ks}})$ where $p = 0.5$. Figures 2C and

2D show the intersection of that hyperplane (dashed) with two-dimensional slices of parameter space. Although we illustrate the concept in two dimensions, the analysis itself is conducted in four dimensions.

Our estimates of the regression coefficients, $\beta_0 = -6.416 \pm .059$, $\beta_{\text{CaL}} = 2.509 \pm .024$, $\beta_{\text{Kr}} = -2.471 \pm .024$, $\beta_{\text{NaL}} = 0.847 \pm .012$, $\beta_{\text{Ks}} = -1.724 \pm .018$, were all statistically significant ($p < .001$). The reported confidence intervals represent ± 1 SE. The model itself was also significantly different from the null model, $\chi^2(99995, n{=}100000) = 73900$, $p < .001$.

The action of drugs in logarithmic coordinates

Drugs attenuate the conductivity of ion channels in a multiplicative fashion. The conductance of the drugged channel is defined as,

$$G_{\text{drug}} = \delta \times G_{\text{ion}},$$

where G_{ion} is the baseline conductance of the ion channel and $\delta \in [0, 1]$ is the fractional conductance imposed by the drug. Logarithmic coordinates transform the action of drug blockade into an additive process,

$$\ln(G_{\text{drug}}) = \ln(\delta) + \ln(G_{\text{ion}}),$$

which can be expressed with vector geometry (Figure 3A). We denote the action of a drug by the vector,

$$\mathbf{A} = \{\alpha_{\text{CaL}}, \alpha_{\text{Kr}}, \alpha_{\text{NaL}}, \alpha_{\text{Ks}}\},$$

where $\alpha = \ln(\delta)$. The values of δ would ordinarily be obtained from patch-clamp experiments. In our case, we calculated them from the published potencies of 109 drugs collated by Llopis-Lorente et al. (2020).

Axis of arrhythmia

We define the axis of arrhythmia as a line that runs orthogonally to the decision boundary (Figure 3A). It represents the shortest path for shifting any cardiomyocyte into the ectopic regime by modifying the conductances of its ion channels. The basis vector of the axis,

$$\mathbf{B} = \{\beta_{\text{CaL}}, \beta_{\text{Kr}}, \beta_{\text{NaL}}, \beta_{\text{Ks}}\},$$

is defined by the coefficients of the regression equation.

Drug risk metric

The arrhythmogenic component of a drug is obtained by projecting the action of the drug onto the axis of arrhythmia. The length of the projection is our metric of drug risk. Specifically,

$$\text{risk} = \frac{\mathbf{A} \cdot \mathbf{B}}{||\mathbf{B}||}, \qquad \textbf{(2)}$$

where $\mathbf{A}$ is the action of the drug, $\mathbf{B}$ is the basis vector of the axis of arrhythmia, and $\mathbf{A} \cdot \mathbf{B} = \sum_i \alpha_i \beta_i$ is the dot product. The metric is normalized to the euclidean length of $\mathbf{B}$, which is denoted $||\mathbf{B}||$. For our estimates of the regression coefficients,

$$\mathbf{B} = \{2.509, -2.471, 0.847, -1.724\}$$

and $||\mathbf{B}|| = \sqrt{\beta_{\text{CaL}}^2 + \beta_{\text{Kr}}^2 + \beta_{\text{NaL}}^2 + \beta_{\text{Ks}}^2} = 4.01$.

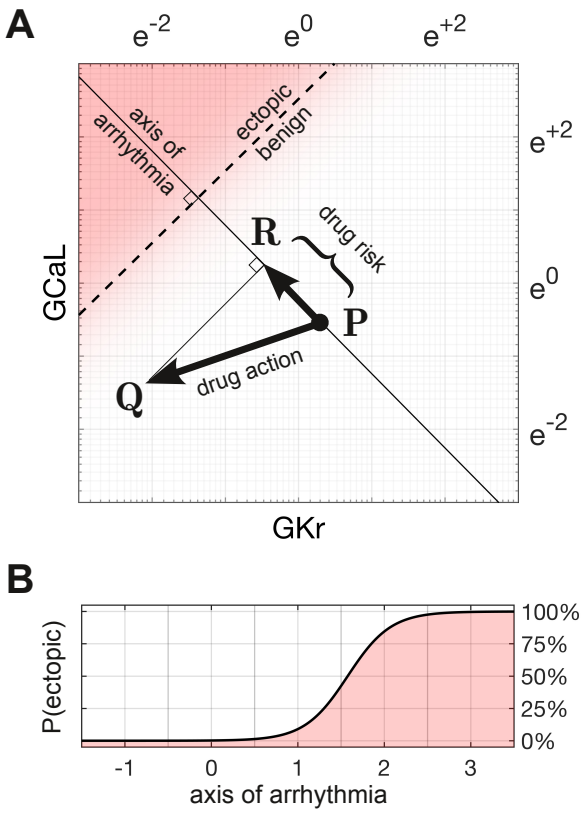

Figure 3. Quantifying drug risk with the axis of arrhythmia. (A) The axis of arrhythmia runs orthogonally to the decision boundary. As such, it describes the shortest pathway to ectopy for any cardiomyocyte. The action of a drug is represented by $\overrightarrow{PQ}$. The arrhythmogenic component of that drug is $\overrightarrow{PR}$. It is obtained by projecting $\overrightarrow{PQ}$ onto the axis of arrhythmia. The length of $\overrightarrow{PR}$ is our measure of drug risk. **(B)** The cross-sectional profile of the decision boundary along the axis of arrhythmia. The origin corresponds to the baseline cardiomyocyte.

Risk scores

According to our risk metric, drugs that shift the electrophysiology *towards* the ectopic region have *positive* scores. Conversely, drugs that shift the electrophysiology *away* from ectopy have *negative* scores. Drugs that do neither have scores near zero.

The *a priori* probability of ectopy

The probability of ectopy along the axis of arrhythmia is,

$$p(x) = \frac{1}{1 + \exp(x)}, \qquad \textbf{(3)}$$

where $x = \beta_0 + \beta_{\text{CaL}} X_{\text{CaL}} + \beta_{\text{Kr}} X_{\text{Kr}} + \beta_{\text{NaL}} X_{\text{NaL}} + \beta_{\text{Ks}} X_{\text{Ks}}$. Eq. (3) is obtained by rearranging Eq. (1). It describes the cross-sectional profile of the decision boundary (Figure 3B). As such, it represents the *a priori* probability of a cardiomyocyte being ectopic, on average, based on its proximity to the decision boundary. The shallow slope of the profile is indicative of the statistical uncertainty in fitting a linear boundary to the data points (Figures 2C,D).

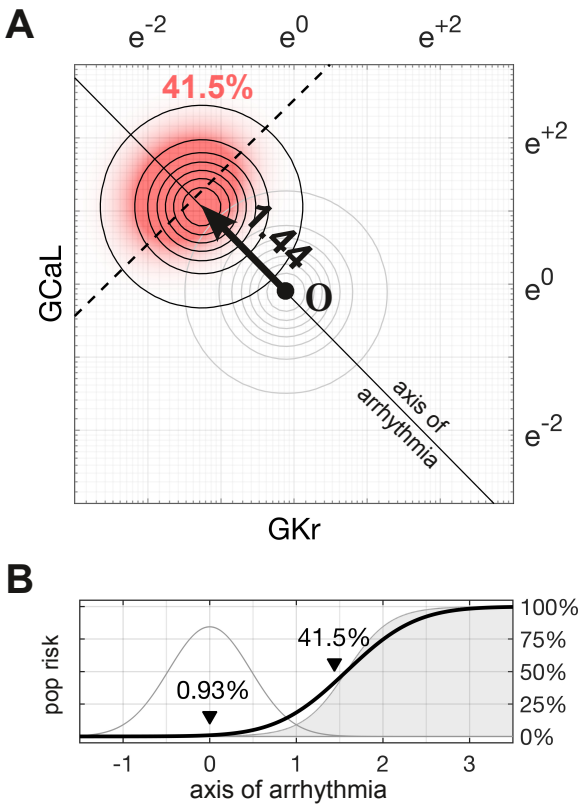

Figure 4. Susceptibility to a drug in the natural population. (A) Natural variation in ion channel conductivity is represented by a symmetric Gaussian density function centered at point $\mathbf{O}$. In this example, a tenfold dose of Ibutilide shifts the population by 1.44 units towards the ecoptic region. The proportion of ectopic myocytes in the drugged population is 41.5% (red). **(B)** The relationship between the drug risk score and ectopy in the natural population. The drug risk score corresponds to position on the axis of arrhythmia. The shaded region is the *a priori* probability of ectopy along that axis (reproduced from Figure 3B). The Gaussian profile (thin gray line) is the natural population density centered at zero. The proportion of myocytes that are ectopic (heavy black line) is 0.93% at baseline. That proportion rises as the drug shifts the population density towards the decision boundary. See Supplementary Video SV1 for an animated version.

Susceptibility in the natural population

A drug alters the electrophysiology of all cardiomyocytes to the same extent but only some cardiomyocytes become ectopic. The most susceptible are those that are closest to the decision boundary. We calculated the proportion of the natural population that would be susceptible to a given drug by analyzing how the drug shifts the population density with respect to the decision boundary.

Following the methods of Sobie (2009), Sadrieh et al. (2013), Morotti and Grandi (2017), Gong and Sobie (2018) we assumed that ion channel conductances varied independently in nature and were log-normally distributed $(\mu = -0.112, \sigma = 0.472)$. By definition, a log-normal distribution maps onto a normal distribution in logarithmic coordinates. The natural population in our parameter space is therefore a symmetric multivariate Gaussian density function (Figure 4A). In the absence of drugs, the natural population density in four dimensions is centered at the point $\mathbf{O} = \{\mu, \mu, \mu, \mu\}$.

The proportion of myocytes that become ectopic depends on how far the population is shifted along the axis of arrhythmia according to the risk metric (Figure 4B). The proportion is calculated as the product of the *a priori* probability of the ectopy (Eq. 3) and the density of the drugged population (Eq. 5; Methods). For the case of 10x therapeutic dose of Ibutilide — a potent blocker of I_{Kr} — the proportion of the natural population that is susceptible to drug-induced Torsades is 41.5% (Figure 4). Since the size of the susceptible population is monotonically related to the drug's risk score, the torsadogenic risk can be described using either terminology.

Validation against known drugs

We used the Hill equation to reconstruct the drug-response profiles of G_{Kr}, G_{CaL}, G_{Ks} and G_{NaL} from the half-maximal inhibitory concentrations (IC_{50}) of 109 drugs reported by Llopis-Lorente et al., 2020. The results for each drug are included in the Supplementary Information. Llopis-Lorente et al. (2020) labeled the clinical risks according to the Credible Meds list of QT drugs (Woosley et al., 2019). In that labeling scheme, Class 1 drugs carry a known torsadogenic risk; Class 2 drugs carry a possible risk; Class 3 drugs carry a risk but only in conjunction with other factors; Class 4 drugs have no evidence of risk at all.

Cases of Ajmaline and Linezolid

Ajmaline is an anti-arrhythmic drug that primarily blocks the fast sodium current (Kiesecker et al., 2004). Clinicians must administer Ajmaline with care because it is also a potent blocker of I_{Kr} (Figure 5A, left) with a known risk of Torsades (Class 1). In comparison, Linezolid is an antibacterial agent that has no clinical evidence of Torsades (Class 4) even though it too blocks I_{Kr}. Albeit less than it blocks I_{CaL} (Figure 5A, right).

Indeed, the two drugs have nearly opposite effects on G_{CaL} and G_{Kr}, as can be seen in the case of 25x therapeutic dose (Figure 5B). Using vector notation, the blocking action of 25x dose of Ajmaline is,

$$\mathbf{A}_{\text{Ajmaline}} = \{-0.425, -2.32, 0, 0\},$$

and the blocking action of Linezolid is,

$$\mathbf{A}_{\text{Linezolid}} = \{-2.71, -0.828, 0, 0\}.$$

The two drugs shift the electrophysiology in opposite directions along the axis of arrhythmia (Figure 5C). The corresponding risk scores are $+1.16$ for Ajmaline and -1.18 for Linezolid. The signs of the scores suggest that Ajmaline is pro-arrhythmic whereas Linezolid is not, which agrees with the clinical risk labels. Indeed, the sizable negative score for Linezolid suggests that it may actually have anti-arrhythmic properties.

The effect of both drugs on the natural population is shown in Figure 5D. Ajmaline shifts the population density by 1.16 units towards the ectopic regime, which suggests that 26% of the recipients would be susceptible

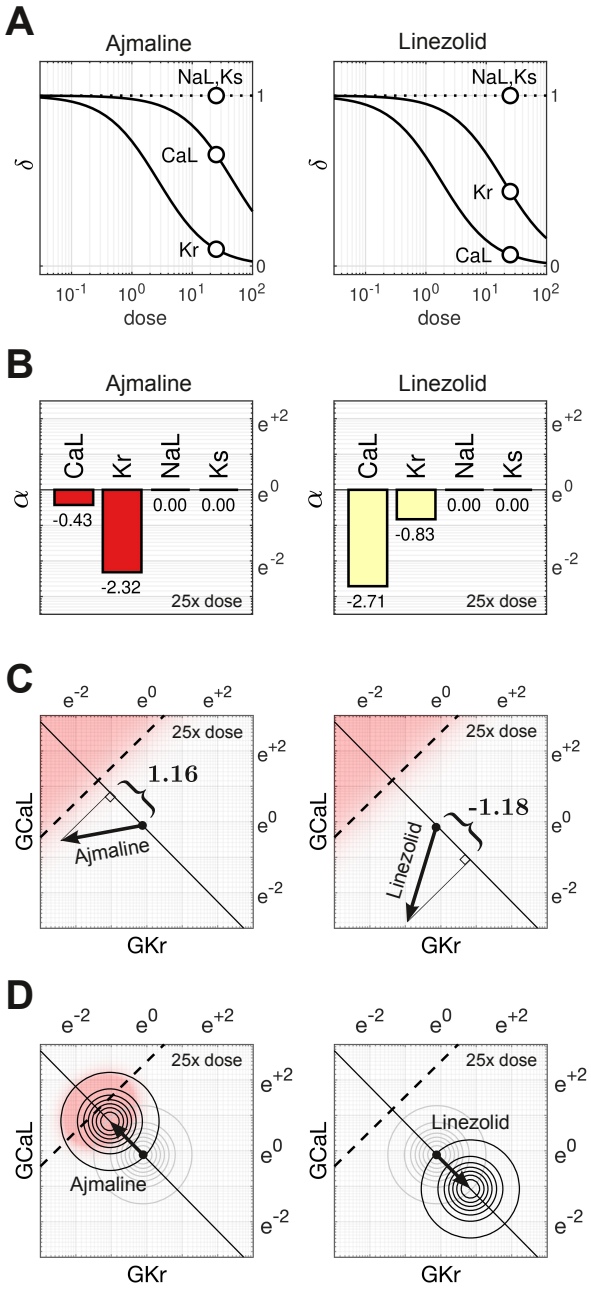

Figure 5. Cases of Ajmaline and Linezolid. (A) Drug response profiles of $I_{\text{CaL}}, I_{\text{Kr}}, I_{\text{NaL}}$ and I_{Ks} relative to the therapeutic dose. Open circles highlight 25x therapeutic dose. Ajmaline has $\delta_{\text{CaL}} = 0.654$ and $\delta_{\text{Kr}} = 0.0986$ at 25x dose, whereas Linezolid has $\delta_{\text{CaL}} = 0.067$ and $\delta_{\text{Kr}} = 0.437$. Data for I_{NaL} and I_{Ks} were not available, so they were assumed to be unaffected ($\delta_{\text{NaL}} = 1$ and $\delta_{\text{Ks}} = 1$). **(B)** The blocking action of Ajmaline and Linezolid at 25x dose. Drug action is defined as $\alpha = \ln(\delta)$. **(C)** The corresponding risk scores for Ajmaline $(+1.16)$ and Linezolid (-1.18) at that dose. **(E)** The drug-induced shifts of the natural population density along the axis of arrhythmia. The proportion of myocytes that are ectopic with 25x dose of Ajmaline is 26% (red), compared to only 0.0095% for Linezolid.

to Torsades. Conversely, Linezolid shifts the population 1.18 units away from the ectopic regime. So only 0.0095% of those who received Linezolid would be susceptible. A substantial drop from the baseline rate of 0.93%.

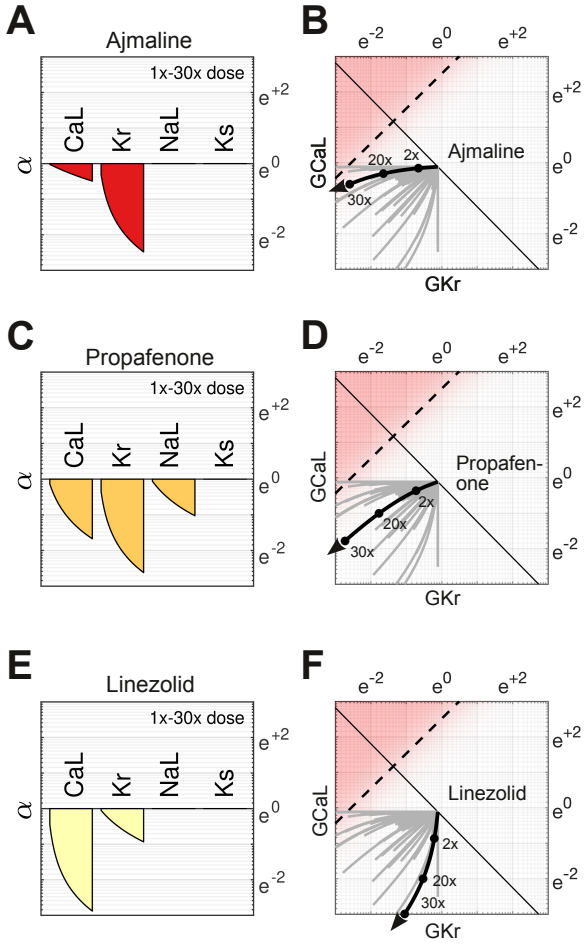

Figure 6. The effect of multi-channel block changes with dosage. (A) The attenuation of G_{CaL}, G_{Kr}, G_{NaL} and G_{Ks} by Ajmaline over a range of doses. **(B)** The action of Ajmaline in parameter space. Gray traces are the pathways of all 109 drugs that we investigated. **(C-D)** Propafenone. **(E-F)** Linezolid.

Drug action varies with dose

The direction of a drug's line of action is liable to vary with dosage because of differential binding to each ion channel. For example, Ajmaline disproportionately blocks more I_{Kr} than I_{CaL} with increasing dosage (Figure 6A). Hence the pathway of Ajmaline follows a gentle arc in parameter space rather than a straight line (Figure 6B). The effect is less pronounced for Propafenone which recruits the ion channels more uniformly (Figure 6C). Nonetheless, its path is still not strictly linear (Figure 6D). Linezolid follows a similar pattern to Ajmaline but in the opposite direction (Figures 6E and 6F). In general, the pathways of all 109 drugs (light gray traces) exhibited a variety of curvatures that influence their projection onto the axis of arrhythmia. Consequently the relative scores of some drugs change subtly with dosage.

Testing the risk metric

The metric was tested by scoring all 109 drugs over a range of doses and comparing the results to the clinical risk labels from Credible Meds. The clinical labels were lumped into two categories for this purpose: UNSAFE (class 1 and 2) versus SAFE (class 3 and 4). Drugs

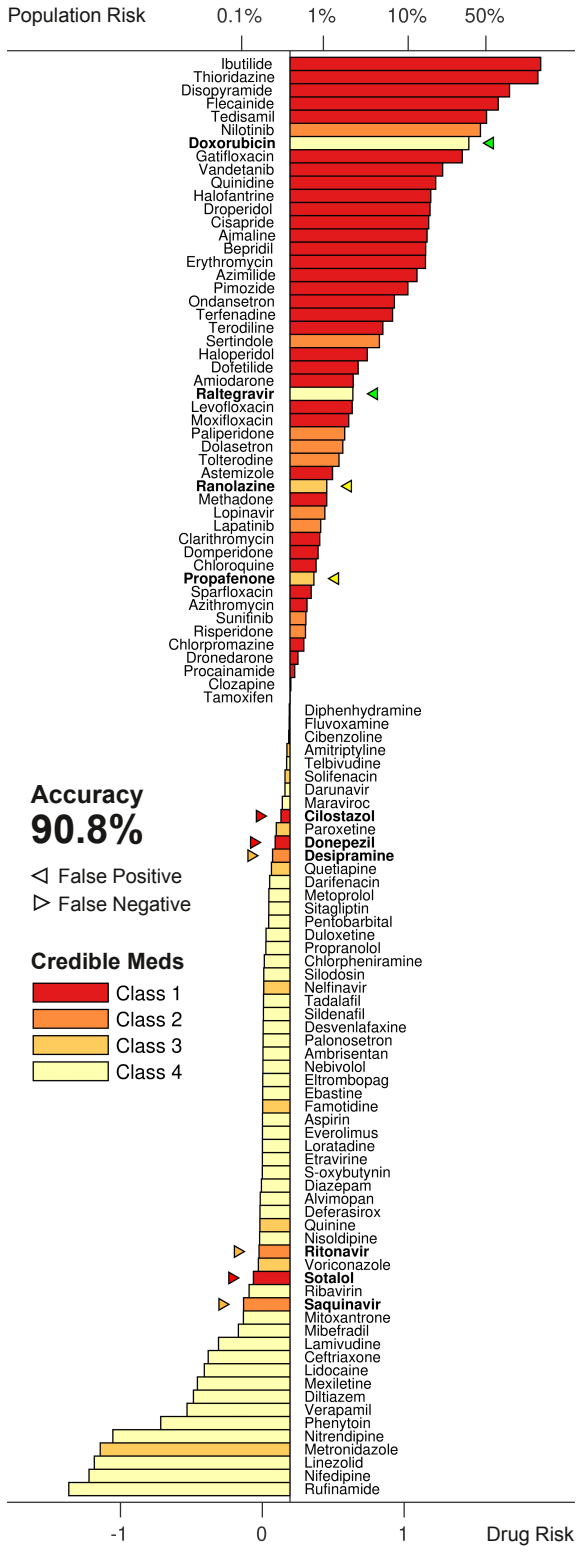

Figure 7. Torsadogenic risk for 109 drugs at 25x dose. Colors indicate the clinical risk labels from Credible Meds. The drugs are sorted by the score returned by our risk metric (lower axis). The proportion of the natural population that would be susceptible to the drug is shown on the upper axis. Drugs to the right of the scoring threshold ($\theta = 0.195$) were classified as UNSAFE and those to the left of it were classified as SAFE. Misclassified drugs are marked with a triangle and highlighted in bold. In this case, 90.8% of the drugs were correctly classified.

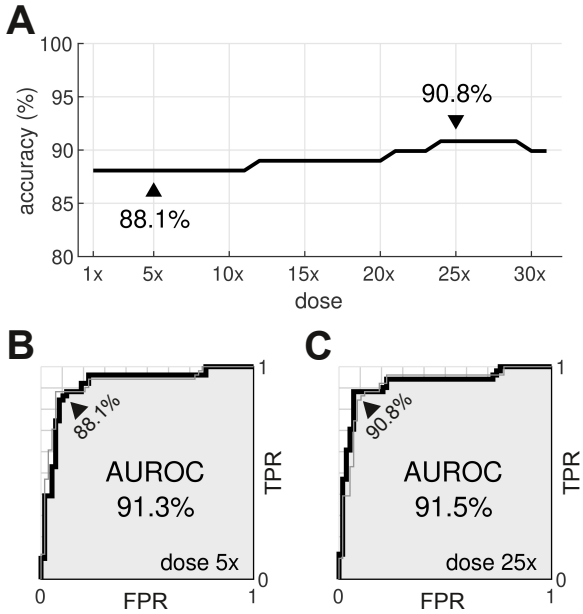

Figure 8. Optimal dosage. (A) Classification accuracy for drugs assessed at a range of dosages. **(A)** ROC curve for drugs at 5x dose. **(B)** ROC curve for drugs at 25x dose. AUROC is area under the ROC curve. TPR is true positive rate. FPR is false positive rate. The false negative rate is 1-TPR.

that scored above a given threshold (risk $> \theta$) were predicted to be UNSAFE and those that scored below the threshold (risk $< \theta$) were predicted to be SAFE. The threshold was optimized for each dosage. For drugs assessed at 25x dose, a classification accuracy of 90.8% was achieved using a scoring threshold of $\theta = 0.195$ (Figure 7).

The procedure was repeated for doses ranging from 1x to 32x. The classification accuracy for all dosage levels was found to lay between 88.1% and 90.8% (Figure 8A). The differences were primarily due to classification errors in a small number of borderline cases. So we refrain from nominating any one dosage as being optimal. The conventional hERG assay, in comparison, has an accuracy of 78.9% with the same dataset (Llopis-Lorente et al., 2020).

From a safety perspective, the trade-off between false negatives and false positives can be tuned by adjusting the scoring threshold, θ. This is illustrated by the Receiver Operating Characteristic (ROC) curves (Figures 8B and 8C). In our case, there is little difference between the ROC curves for drugs assessed at 5x dose versus 25x dose. The area under the ROC curves (AUROC) are nearly identical at 91.3% and 91.5% respectively. In comparison, the conventional hERG assay has an AUROC of $77 \pm 7\%$ (Kramer et al., 2013).

Discussion

In this study we have proposed a new metric of torsadogenic risk that is based on the axis of arrhythmia. The major benefit of the metric is that it can be applied to novel drugs without conducting any new computer simulations. The drug response profiles of four ion currents

$(\delta_{\text{CaL}}, \delta_{\text{Kr}}, \delta_{\text{NaL}}, \delta_{\text{Ks}})$ are all that is needed to calculate the torsadogenic risk of the drug. The ion currents can be measured using standard patch clamp techniques and the risk metric can be calculated with pen and paper. This simplicity removes a technological hurdle to the adoption of computational assays in safety pharmacology.

Identifying the axis of arrhythmia

All of the simulations in the present study were conducted in the absence of drugs. They were only needed to identify the axis of arrhythmia and do not need to be repeated when applying the metric. The axis encapsulates the linear relationship between the four ion channels and the onset of early after-depolarizations. It corresponds to the most potent combination of pro-arrhythmic drug block that is theoretically possible. The assumption of linearity is crucial for averaging the risk across all individuals. So even though a nonlinear decision boundary might fit the data better, it would not be helpful because the results would be patient specific.

Susceptibility to drug-induced arrhythmia

Our method can also predict the proportion of the population that would be susceptible to a drug without explicitly simulating it. The analysis is possible because drug blockade and natural diversity both operate on the same properties of ion channels. The two biological processes are therefore mathematically interchangeable. As such, the distribution of the drugged population can be inferred from the drug-free population by shifting it according to the drug's risk score. The size of the susceptible population is a function of the risk score. So the torsadogenic risk can be reported either as a raw score or as a percentage of the population at risk.

Comparison to conventional approaches

Conventional *in silico* safety assays are designed to apply the drug directly to simulated cardiomyocytes and then use biomarkers in the action potential to predict the torsadogenic risk. See Grandi et al. (2018) for a review. The predictions are optimized for established drugs using a training procedure that has been formalized by the Comprehensive In Vitro Proarrhythmia Assay (CiPA) initiative (Colatsky et al., 2016). The CiPA steering committee (Li et al., 2019) recommends the CiPAORdv1.0 variant of the O'Hara-Rudy model which incorporates the kinetics of drugs binding with the hERG channel (Li et al., 2017). The recommended biomarker is qNet (Dutta et al., 2017) which measures the net charge of six major ion currents $(I_{\text{Kr}}, I_{\text{CaL}}, I_{\text{NaL}}, I_{\text{to}}, I_{\text{Ks}}, I_{\text{K1}})$. The clinical risks of the CiPA drugs (n=28) are labeled low, intermediate or high. *Low* versus *intermediate-or-high* risk drugs were predicted with 84–95% accuracy using manual patch clamp techniques; or 93-100% accuracy using automated patch clamping (Li et al., 2019). Whereas *low-or-intermediate* versus *high* risk drugs were predicted to 92–100% accuracy using manual patch clamp; or 88-98% using automated patch clamp (Li et al., 2019). The measurement of the drug potencies is a source of considerable variability, which is exacerbated by the small number of test drugs (n=16). The accuracy ranges reported by Li et al. (2019) appear to outperform our results, although they cannot be compared directly because the risk labels are stratified very differently.

Passini et al. (2017) used a larger dataset (n=62) to obtain 89% accuracy at predicting class 1 versus class 2–4 torsadogenic risk labels from Credible Meds. The cardiomyocytes were simulated using the baseline O'Hara-Rudy model without dynamic drug-binding kinetics. The accuracy is within the range of our results, albeit using a slightly different risk stratification scheme. Passini et al. (2017) scored the torsadogenic risk independently of dosage by averaging number of early after-depolarizations, weighted by the concentration of the drug. However we believe it is better to quantify the risk as a function of dosage, since even the most lethal drug is safe at zero dose.

The present study uses the same dataset (n=109) as Llopis-Lorente et al. (2020) who investigated a suite of biomarkers using a recalibrated O'Hara-Rudy model which also had revised gating kinetics for I_{Na}. Their best performing biomarker was qNet, which predicted class 1–2 versus class 3–4 torsadogenic risk with 92.7% accuracy. It exceeds our best result by approximately 2% on the same risk stratification scheme. Llopis-Lorente et al. (2020) increased the overall performance to 94.5% by combining the best biomarkers into a decision tree. Interestingly, early after-depolarizations proved to be their worst biomarker with only 78.9% accuracy. Based on our analysis, it is likely they undersampled the early after-depolarizations by constraining their cardiomyocytes to normal physiological limits.

Comparison to MICE models

MICE models (Kramer et al., 2013) use logistic regression to predict the torsadogenic risk of a drug directly from the half maximal inhibitory concentrations (IC_{50}) for hERG, Cav1.2 and Nav1.5. They are derived using statistical model fitting techniques. Kramer et al. (2013) trained six candidate models on a dataset of 55 drugs. Their best model was found to predict the torsadogenic labels of the drugs with 90.9% accuracy using only the difference between hERG and Cav1.2. Specifically,

$$\ln \frac{p}{1-p} = \beta_0 + \beta_1 (C - H),$$

where $H = -\ln(IC_{50})$ for hERG, and $C = -\ln(IC_{50})$ for Cav1.2. The form of the predictor variables are strikingly similar to our own except that we use the fractional conductance (δ) instead of IC_{50}. In our case, the predictors were derived from biophysical principals of drug block rather than through statistical model fitting. The accuracy of the two models are nearly identical, albeit on different datasets.

Comparison to Bnet

Bnet (Mistry, 2018) is a simple linear model that predicts the torsadogenic risk of a drug directly from the net blockade of inward and outward ion currents. Notably,

$$B_{net} = \sum_{i}^{n} R_r - \sum_{j}^{m} D_j$$

where R_i and D_j represent the percentage block of the repolarizing currents $(I_{\text{Kr}}, I_{\text{Ks}}, I_{\text{to}})$ and the depolarizing currents $(I_{\text{CaL}}, I_{\text{Na}}, I_{\text{NaL}}, I_{\text{K1}})$ respectively. Percentage block is akin to $(1-\delta)$ in our model but without the logarithmic transform that we use to analyze attenuation as an additive process. Bnet predicts the clinical risk labels of the CiPA validation drugs just as well as the CiPAORdv1.0 model when adjusted for drug binding kinetics (Li et al., 2019; Mistry, 2019; Han et al., 2019). This has opened a debate between model complexity and biophysical realism in which proponents of biophysical models advocate their explanatory benefits (Lancaster and Sobie, 2017), whereas proponents of simple models advocate their predictive power without the computational expense (Mistry et al., 2015; Mistry, 2017).

Conclusion

Our approach resolves the debate between model complexity and biophysical realism by combining both approaches into the same enterprise. The method is initiated using biophysical models to explore the relationship between ion channels and torsadogenic risk — as it is best understood by theory. The findings are then condensed into a simple linear model that can be applied without recapitulating the biophysical details. That is not to say the linear model is mere statistical correlation. It still represents the biophysical action of multichannel drug blockade but only as far as it relates to early after-depolarizations. Our approach thus represents a convergence of biophysical and simple models. One that provides the benefits of biophysical modeling without the computational burden. We believe it will accelerate the adoption of computational assays in safety pharmacology and ultimately reduce the burden of animal testing.

Methods

The action potentials of human endocardial ventricular cardiomyocytes were simulated using a variant of the ORD11 model (O'Hara et al., 2011) in which the maximal conductances of G_{Ks}, G_{Kr}, G_{CaL}, G_{NaL}, P_{NaCa} and P_{NaK} were re-scaled (Table 1) to better reproduce the clinical phenotypes of long QT syndrome (Mann et al., 2016; Krogh-Madsen et al., 2017). The source code for the ORD11 model (O'Hara et al., 2011) was adapted to run in the Brain Dynamics Toolbox (Heitmann et al., 2018; Heitmann and Breakspear, 2022). The adapted source code is available from Heitmann (2023). The differential equations were integrated forward in time using the matlab `ode15s` solver with error tolerances `AbsTol=1e-3` and `RelTol=1e-6`. The model was paced at 1 Hz with a stimulus of -70 mV and duration of 0.5 ms. All simulations were equilibrated for at least 1000 beats prior to analysis.

Maximal Conductance	Multiplier
G_{Ks}	8.09
G_{Kr}	1.17
G_{CaL} (P_{Ca})	3.57
P_{NaCa}	3.05
P_{NaK}	1.91
G_{NaL}	1.7

Table 1. The baseline scaling factors applied to the ORD11 model.

Classification of ectopic phenotypes

Blocks of four successive beats were analyzed to accommodate alternans. Cells were classified as ectopic if any of those four beats contained an early after-depolarization — as defined by any secondary peak that rose above -50 mV and was separated from other peaks by at least 100 ms. Cells that did not exhibit early after-depolarizations were classified as benign.

Parameter domain

We chose the domain of parameter space $(G \in e^{\pm 3})$ using trial and error. The domain must be large enough to cover the ectopic region but not so large as to be unduly influenced by biological extremes. Our chosen domain spans conductances between 0.05 and 20 times their baseline value.

Natural population density

Cell-to-cell variability was mimicked by scaling the conductances $(G_{\text{CaL}}, G_{\text{Kr}}, G_{\text{NaL}}, G_{\text{Ks}})$ by a random multiplier that was drawn from a log-normal distribution (Sobie, 2009). The parameters of the distribution $(\mu{=}0.112, \sigma = 0.472)$ were chosen to give the multipliers a mean of 1 and standard deviation of 0.5. The spread was based on our experience with previous simulations (Sadrieh et al., 2013, 2014; Ballouz et al., 2020; TeBay et al., 2022). The four ion channel species were assumed to vary independently.

By definition, the log-normal distribution maps onto the normal distribution under the logarithmic transform. The natural population was therefore represented in logarithmic parameter space by a symmetric multivariate normal distribution. Specifically,

$$f(w,x,y,z) = f(w)\,f(x)\,f(y)\,f(z),$$

where

$$f(x) = \frac{1}{\sqrt{2\pi\sigma^2}} \exp\left(-\frac{(x-\mu)^2}{2\sigma^2}\right) \qquad \textbf{(4)}$$

is the univariate normal distribution.

Joint probability

Rotational symmetry allowed the multivariate distribution to be projected onto the axis of arrhythmia as a univariate distribution. The probability of a cardiomyocyte in the natural population being ectopic is,

$$P = \int p(x)\, f(x)\, dx, \tag{5}$$

where $p(x)$ is the *a priori* probability of ectopy for that phenotype (Eq. 3) and $f(x)$ is the proportion of cells in the population with that phenotype (Eq. 4). Drugs serve to shift $f(x)$ along the axis of arrhythmia. The size of that shift is defined by the risk metric (Eq. 2).

Drug dataset

The drug response curves were reconstructed using the Hill equation,

$$\delta = \frac{\mathrm{IC}_{50}^{h}}{\mathrm{IC}_{50}^{h} + [C]^{h}},$$

where $\delta \in [0, 1]$ represents the fractional conductance of the ion channel. The concentration of the drug (C) was normalized to the effective free therapeutic plasma concentration (EFTPC). The Hill coefficient was fixed at $h = 1$ on the assumption that single drug molecules bound to the ion channels independently. The half-maximal inhibitory concentrations (IC_{50}) were taken from Supplementary Table S2 of Llopis-Lorente et al. (2020). That data was curated from multiple public databases and scientific publications to ameliorate the effects of cross-site and cross-platform variability (Kramer et al., 2020). The dataset uses the median IC_{50} for cases where multiple values were reported (Llopis-Lorente et al., 2020). Similarly, it uses the highest therapeutic dosage for cases where multiple EFTPCs were reported (Llopis-Lorente et al., 2020). Ion channels with missing IC_{50} values were assumed not to be blocked by the drug $(\delta = 1)$. The reconstructed response curves are given in Supplementary Dataset S1. The clinical risk labels for the drugs were transcribed from Table 1 of Llopis-Lorente et al. (2020).

Acknowledgments

This study was supported by Australian NHMRC grants app1182032, app1182623 and NSW Health cardiovascular capacity building grant. SH was also funded by The Medical Advances Without Animals Trust (MAWA). The aim of MAWA is to advance medical science and improve human health and therapeutic interventions without the use of animals or animal products. This research includes computations using the computational cluster Katana supported by Research Technology Services at UNSW Sydney.

Ballouz, S., Mangala, M. M., Perry, M. D., Heitmann, S., Gillis, J. A., Hill, A. P., and Vandenberg, J. I. Co-expression of calcium and hERG potassium channels reduces the incidence of proarrhythmic events. *Cardiovascular Research*, (cvaa280), Oct. 2020. doi: 10.1093/cvr/cvaa280.

Britton, O. J., Bueno-Orovio, A., Van Ammel, K., Lu, H. R., Towart, R., Gallacher, D. J., and Rodriguez, B. Experimentally calibrated population of models predicts and explains intersubject variability in cardiac cellular electrophysiology. *PNAS*, 110(23):E2098–E2105, June 2013. doi: 10.1073/pnas.1304382110.

Colatsky, T., Fermini, B., Gintant, G., Pierson, J. B., Sager, P., Sekino, Y., Strauss, D. G., and Stockbridge, N. The Comprehensive in Vitro Proarrhythmia Assay (CiPA) initiative — Update on progress. *J Pharmacol Toxicol Methods*, 81:15–20, Sept. 2016. doi: 10.1016/j.vascn.2016.06.002.

Dutta, S., Chang, K. C., Beattie, K. A., Sheng, J., Tran, P. N., Wu, W. W., Wu, M., Strauss, D. G., Colatsky, T., and Li, Z. Optimization of an In silico Cardiac Cell Model for Proarrhythmia Risk Assessment. *Front Physiol*, 8:616, 2017. doi: 10.3389/fphys.2017.00616.

Gong, J. Q. X. and Sobie, E. A. Population-based mechanistic modeling allows for quantitative predictions of drug responses across cell types. *NPJ Syst Biol Appl*, 4(1):1–11, Feb. 2018. doi: 10.1038/s41540-018-0047-2. Number: 1 Publisher: Nature Publishing Group.

Grandi, E., Morotti, S., Pueyo, E., and Rodriguez, B., editors. *Safety Pharmacology - Risk Assessment QT Interval Prolongation and Beyond*. Frontiers Research Topics. Frontiers Media SA, 2018. ISBN 978-2-88945-539-3. doi: 10.3389/978-2-88945-539-3.

Han, S., Han, S., Kim, K.-S., Lee, H.-A., and Yim, D.-S. Usefulness of Bnet, a Simple Linear Metric in Discerning Torsades De Pointes Risks in 28 CiPA Drugs. *Front Pharmacol*, 10, 2019.

Heitmann, S. and Breakspear, M. *Handbook for the Brain Dynamics Toolbox: Version 2022*. bdtoolbox.org, 7th edition, 2022. ISBN 978-0-645-06692-0.

Heitmann, S., Aburn, M. J., and Breakspear, M. The Brain Dynamics Toolbox for Matlab. *Neurocomputing*, 315:82–88, Nov. 2018. doi: 10.1016/j.neucom.2018.06.026.

Heitmann, S. Source code for simulating the O'Hara-Rudy (ORd) model of the human cardiac action potential in the Brain Dynamics Toolbox, Apr. 2023. URL https://zenodo.org/record/7796721.

Hoffmann, P. and Warner, B. Are hERG channel inhibition and QT interval prolongation all there is in drug-induced torsadogenesis? A review of emerging trends. *J Pharmacol Toxicol Methods*, 53(2):87–105, Mar. 2006. doi: 10.1016/j.vascn.2005.07.003.

Hondeghem, L. M. TRIad: Foundation for Proarrhythmia (Triangulation, Reverse Use Dependence and Instability). In *The hERG Cardiac Potassium Channel: Structure, Function and Long QT Syndrome*, pages 235–250. John Wiley & Sons, Ltd, 2005. ISBN 978-0-470-02142-2.

ICH Harmonised Tripartite Guideline. The non-clinical evaluation of the potential for delayed ventricular repolarization (QT Interval Prolongation) by human pharmaceuticals S7B. 2005.

Kiesecker, C., Zitron, E., Lück, S., Bloehs, R., Scholz, E. P., Kathöfer, S., Thomas, D., Kreye, V. A. W., Katus, H. A., Schoels, W., Karle, C. A., and Kiehn, J. Class Ia anti-arrhythmic drug ajmaline blocks HERG potassium channels: mode of action. *Naunyn-Schmiedeberg's Arch Pharmacol*, 370(6):423–435, Dec. 2004. doi: 10.1007/s00210-004-0976-8.

Kramer, J., Obejero-Paz, C. A., Myatt, G., Kuryshev, Y. A., Bruening-Wright, A., Verducci, J. S., and Brown, A. M. MICE Models: Superior to the HERG Model in Predicting Torsade de Pointes. *Sci Rep*, 3(1):2100, Dec. 2013. doi: 10.1038/srep02100.

Kramer, J., Himmel, H. M., Lindqvist, A., Stoelzle-Feix, S., Chaudhary, K. W., Li, D., Bohme, G. A., Bridgland-Taylor, M., Hebeisen, S., Fan, J., Renganathan, M., Imredy, J., Humphries, E. S. A., Brinkwirth, N., Strassmaier, T., Ohtsuki, A., Danker, T., Vanoye, C., Polonchuk, L., Fermini, B., Pierson, J. B., and Gintant, G. Cross-site and cross-platform variability of automated patch clamp assessments of drug effects on human cardiac currents in recombinant cells. *Sci Rep*, 10(1):5627, Mar. 2020. doi: 10.1038/s41598-020-62344-w. Number: 1 Publisher: Nature Publishing Group.

Krogh-Madsen, T., Jacobson, A. F., Ortega, F. A., and Christini, D. J. Global Optimization of Ventricular Myocyte Model to Multi-Variable Objective Improves Predictions of Drug-Induced Torsades de Pointes. *Front. Physiol.*, 8:1059, Dec. 2017. doi: 10.3389/fphys.2017.01059.

Lancaster, M. C. and Sobie, E. Improved Prediction of Drug-Induced Torsades de Pointes Through Simulations of Dynamics and Machine Learning Algorithms. *Clin. Pharmacol. Ther.*, 100(4):371–379, 2016. doi: 10.1002/cpt.367.

Lancaster, M. and Sobie, E. Response to "Complexity vs. Simplicity: The Winner Is?" Mechanism-Based Classifiers Provide More Than Just Classification. *Clin. Pharmacol. Ther.*, 101(3):327–327, Mar. 2017. doi: 10.1002/cpt.500.

Li, Z., Dutta, S., Sheng, J., Tran, P. N., Wu, W., Chang, K., Mdluli, T., Strauss, D. G., and Colatsky, T. Improving the In Silico Assessment of Proarrhythmia Risk by Combining hERG (Human Ether-à-go-go-Related Gene) Channel–Drug Binding Kinetics and Multichannel Pharmacology. *Circ Arrhythm Electrophysiol*, 10(2):e004628, Feb. 2017. doi: 10.1161/CIRCEP.116.004628. Publisher: American Heart Association.

Li, Z., Ridder, B. J., Han, X., Wu, W. W., Sheng, J., Tran, P. N., Wu, M., Randolph, A., Johnstone, R. H., Mirams, G. R., Kuryshev, Y., Kramer, J., Wu, C., Crumb Jr., W. J., and Strauss, D. G. Assessment of an In Silico Mechanistic Model for Proarrhythmia Risk Prediction Under the CiPA Initiative. *Clin. Pharmacol. Ther.*, 105(2):466–475, 2019. doi: 10.1002/cpt.1184.

Llopis-Lorente, J., Gomis-Tena, J., Cano, J., Romero, L., Saiz, J., and Trenor, B. In Silico Classifiers for the Assessment of Drug Proarrhythmicity. *J. Chem. Inf. Model.*, 60(10):5172–5187, Oct. 2020. doi: 10.1021/acs.jcim.0c00201.

Mann, S. A., Imtiaz, M., Winbo, A., Rydberg, A., Perry, M. D., Couderc, J.-P., Polonsky, B., McNitt, S., Zareba, W., Hill, A. P., and Vandenberg, J. I. Convergence of models of human ventricular myocyte electrophysiology after global optimization to recapitulate clinical long QT phenotypes. *J Mol Cell Cardiol*, 100:25–34, Nov. 2016. doi: 10.1016/j.yjmcc.2016.09.011.

Martin, R. L., McDermott, J. S., Salmen, H. J., Palmatier, J., Cox, B. F., and Gintant, G. A. The Utility of hERG and Repolarization Assays in Evaluating Delayed Cardiac Repolarization: Influence of Multi-Channel Block. *J Cardiovasc Pharmacol*, 43(3):369, Mar. 2004.

Mirams, G. R., Cui, Y., Sher, A., Fink, M., Cooper, J., Heath, B. M., McMahon, N. C., Gavaghan, D. J., and Noble, D. Simulation of multiple ion channel block provides improved

early prediction of compounds' clinical torsadogenic risk. *Cardiovascular Research*, 91 (1):53–61, July 2011. doi: 10.1093/cvr/cvr044.

Mistry, H. B., Davies, M. R., and Di Veroli, G. Y. A new classifier-based strategy for in-silico ion-channel cardiac drug safety assessment. *Front Pharmacol*, 6, 2015.

Mistry, H. B. Complexity vs. Simplicity: The Winner Is? *Clin. Pharmacol. Ther.*, 101(3): 326–326, Mar. 2017. doi: 10.1002/cpt.503.

Mistry, H. B. Complex versus simple models: ion-channel cardiac toxicity prediction. *PeerJ*, 6:e4352, Feb. 2018. doi: 10.7717/peerj.4352.

Mistry, H. B. Comprehensive *In Vitro* Proarrhythmic Assay Complexity Bias. *Clin. Pharmacol. Ther.*, 105(6):1323–1324, June 2019. doi: 10.1002/cpt.1400.

Morotti, S. and Grandi, E. Logistic regression analysis of populations of electrophysiological models to assess proarrythmic risk. *MethodsX*, 4:25–34, Jan. 2017. doi: 10.1016/j.mex.2016.12.002.

Ni, H., Morotti, S., and Grandi, E. A heart for diversity: simulating variability in cardiac arrhythmia research. *Front Physiol*, 9:958, 2018. Publisher: Frontiers.

O'Hara, T., Virág, L., Varró, A., and Rudy, Y. Simulation of the Undiseased Human Cardiac Ventricular Action Potential: Model Formulation and Experimental Validation. *PLoS Comput Biol*, 7(5):e1002061, May 2011. doi: 10.1371/journal.pcbi.1002061.

Passini, E., Britton, O. J., Lu, H. R., Rohrbacher, J., Hermans, A. N., Gallacher, D. J., Greig, R. J. H., Bueno-Orovio, A., and Rodriguez, B. Human In Silico Drug Trials Demonstrate Higher Accuracy than Animal Models in Predicting Clinical Pro-Arrhythmic Cardiotoxicity. *Front Physiol*, 8:668, 2017. doi: 10.3389/fphys.2017.00668.

Pugsley, M. K., Authier, S., and Curtis, M. J. Principles of Safety Pharmacology. *Br J Pharmacol*, 154(7):1382–1399, 2008. doi: 10.1038/bjp.2008.280.

Sadrieh, A., Mann, S. A., Subbiah, R. N., Domanski, L., Taylor, J. A., Vandenberg, J. I., and Hill, A. P. Quantifying the origins of population variability in cardiac electrical activity through sensitivity analysis of the electrocardiogram: Sensitivity analysis of ECG signals. *J Physiol*, 591(17):4207–4222, Sept. 2013. doi: 10.1113/jphysiol.2013.251710.

Sadrieh, A., Domanski, L., Pitt-Francis, J., Mann, S. A., Hodkinson, E. C., Ng, C.-A., Perry, M. D., Taylor, J. A., Gavaghan, D., Subbiah, R. N., Vandenberg, J. I., and Hill, A. P. Multiscale cardiac modelling reveals the origins of notched T waves in long QT syndrome type 2. *Nat Commun*, 5(1), Dec. 2014. doi: 10.1038/ncomms6069.

Sobie, E. A. Parameter sensitivity analysis in electrophysiological models using multivariable regression. *Biophys J*, 96(4):1264–1274, 2009. Publisher: Elsevier.

TeBay, C., McArthur, J. R., Mangala, M., Kerr, N., Heitmann, S., Perry, M. D., Windley, M. J., Vandenberg, J. I., and Hill, A. P. Pathophysiological metabolic changes associated with disease modify the proarrhythmic risk profile of drugs with potential to prolong repolarisation. *Br J Pharmacol*, 179(11):2631–2646, June 2022. doi: 10.1111/bph.15757.

Varshneya, M., Mei, X., and Sobie, E. A. Prediction of arrhythmia susceptibility through mathematical modeling and machine learning. *PNAS*, 118(37):e2104019118, Sept. 2021. doi: 10.1073/pnas.2104019118.

Witchel, H. J. Drug-induced hERG Block and Long QT Syndrome. *Cardiovasc Ther*, 29(4): 251–259, 2011. doi: 10.1111/j.1755-5922.2010.00154.x.

Woosley, R. L., Heise, C., Gallo, T., Woosley, D., and Romero, K. A. Risk categories for drugs that prolong QT and induce Torsade de Pointes (TdP), 2019. URL https://www.crediblemeds.org/.

Yap, Y. G. and Camm, A. J. Drug induced QT prolongation and torsades de pointes. *Heart*, 89(11):1363–1372, Nov. 2003. doi: 10.1136/heart.89.11.1363. Publisher: BMJ Publishing Group Ltd Section: Education in Heart.

Supplementary Videos

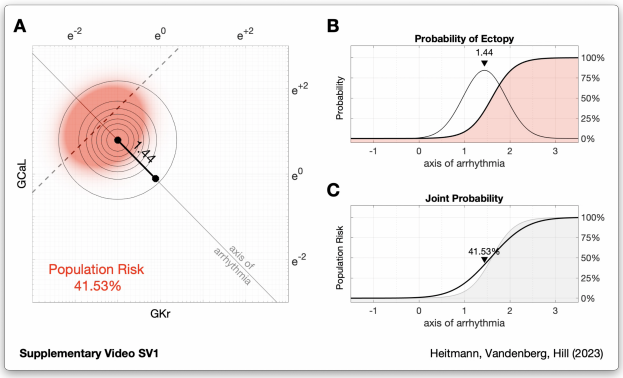

Supplementary Video SV1. Animation of Figure 4 illustrating the relationship between drug risk and population risk. **A.** Drug-induced shift of the the natural population along the axis of arrhythmia. The size of the shift corresponds to the risk score of the drug. **B.** The *a priori* probability of ectopy along the axis of arrhythmia (shaded) in conjunction with the natural population density (light gray). **C.** The probability of ectopy for the natural population (black line) against the *a priori* probability of ectopy (shaded).

Supplementary Information

Supplementary Dataset S1

The drug response data in CSV format. The data was reconstructed from the IC_{50} values published in Supplementary Table S2 of Llopis-Lorente et al (2020). The Hill coefficient was assumed to be $h = 1$ in all cases. Ion channels with missing values were assumed to be unaffected by the drug $(\delta = 1)$. The clinical risk labels were transcribed from Table 1 of Llopis-Lorente et al (2020).

Variable Name	Description
DrugID	Unique identifier for each compound.
Compound	Name of the compound.
Class	Clinical risk label. Class 1 is known risk. Class 2 is possible risk. Class 3 is conditional risk. Class 4 is no evidence of risk.
EFTPC	Effective free therapeutic plasma concentration (nM).
Cmax	Concentration relative to therapeutic dose.
Conc	Concentration of the dose (nM).
GKrScale	Fractional conductance (δ_{Kr}).
GNaScale	Fractional conductance (δ_{Na}).
GNaLScale	Fractional conductance (δ_{NaL}).
GCaLScale	Fractional conductance (δ_{CaL}).
GKsScale	Fractional conductance (δ_{Ks}).
GK1Scale	Fractional conductance (δ_{K1}).
GtoScale	Fractional conductance (δ_{to}).
LogGKrScale	Logarithm of the fractional conductance (α_{Kr}).
LogGNaScale	Logarithm of the fractional conductance (α_{Na}).
LogGNaLScale	Logarithm of the fractional conductance (α_{NaL}).
LogGCaLScale	Logarithm of the fractional conductance (α_{CaL}).
LogGKsScale	Logarithm of the fractional conductance (α_{Ks}).
LogGK1Scale	Logarithm of the fractional conductance (α_{K1}).
LogGtoScale	Logarithm of the fractional conductance (α_{to}).
Score	Torsadogenic risk score where $\mathbf{B} = \{2.509, -2.471, 0.847, -1.724\}$ and $\|\|\mathbf{B}\|\| = 4.01$.

Drugs with Class 1 Torsadogenic risk

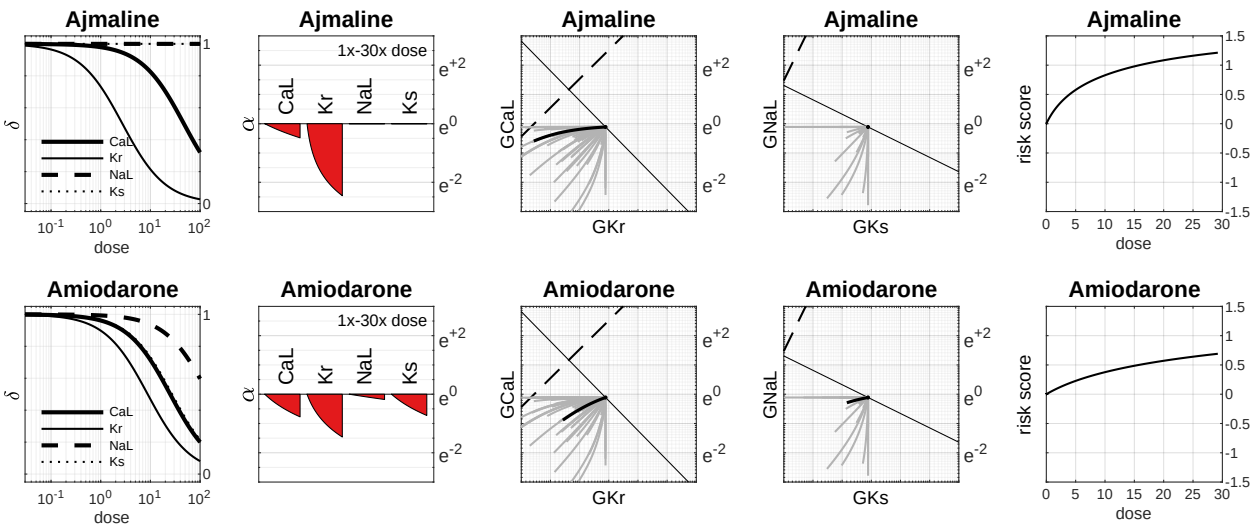

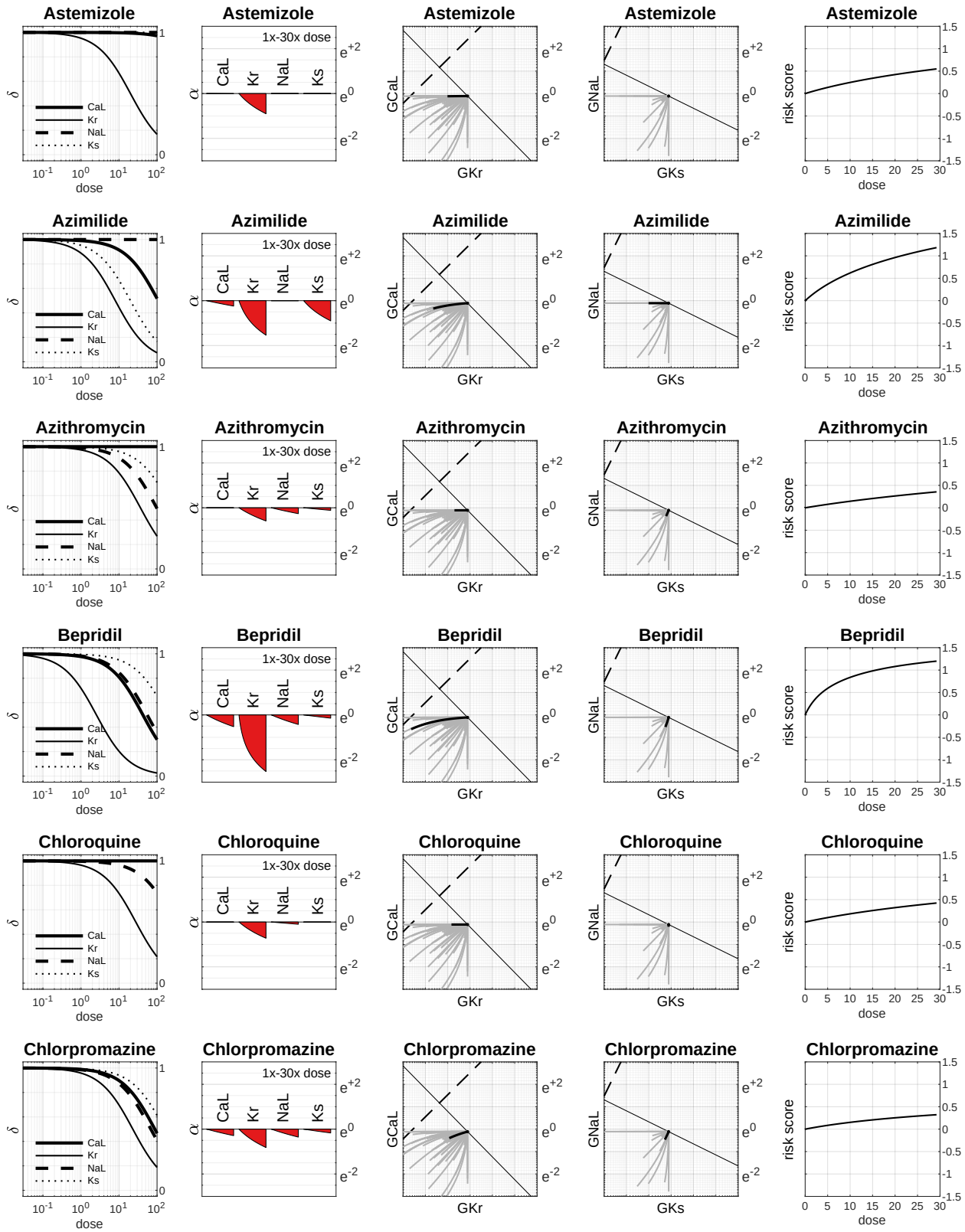
Astemizole
Azimilide
Azithromycin
Bepridil
Chloroquine
Chlorpromazine
δ
dose
CaL
Kr
NaL
Ks
1x-30x dose
α
GCaL
GKr
GNaL
GKs
risk score

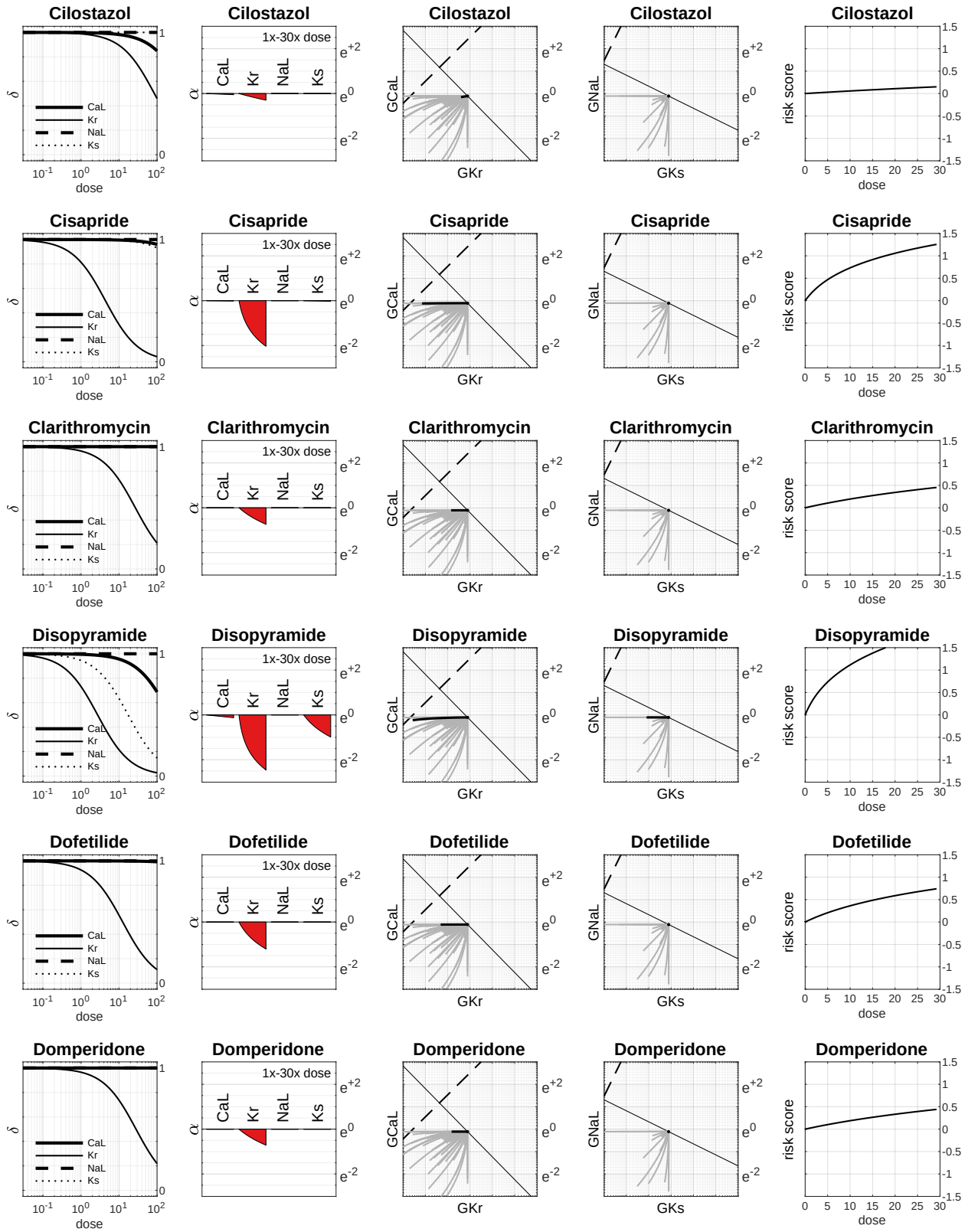
Cilostazol
Cisapride
Clarithromycin
Disopyramide
Dofetilide
Domperidone
δ
dose
CaL
Kr
NaL
Ks
1x-30x dose
α
GCaL
GKr
GNaL
GKs
risk score

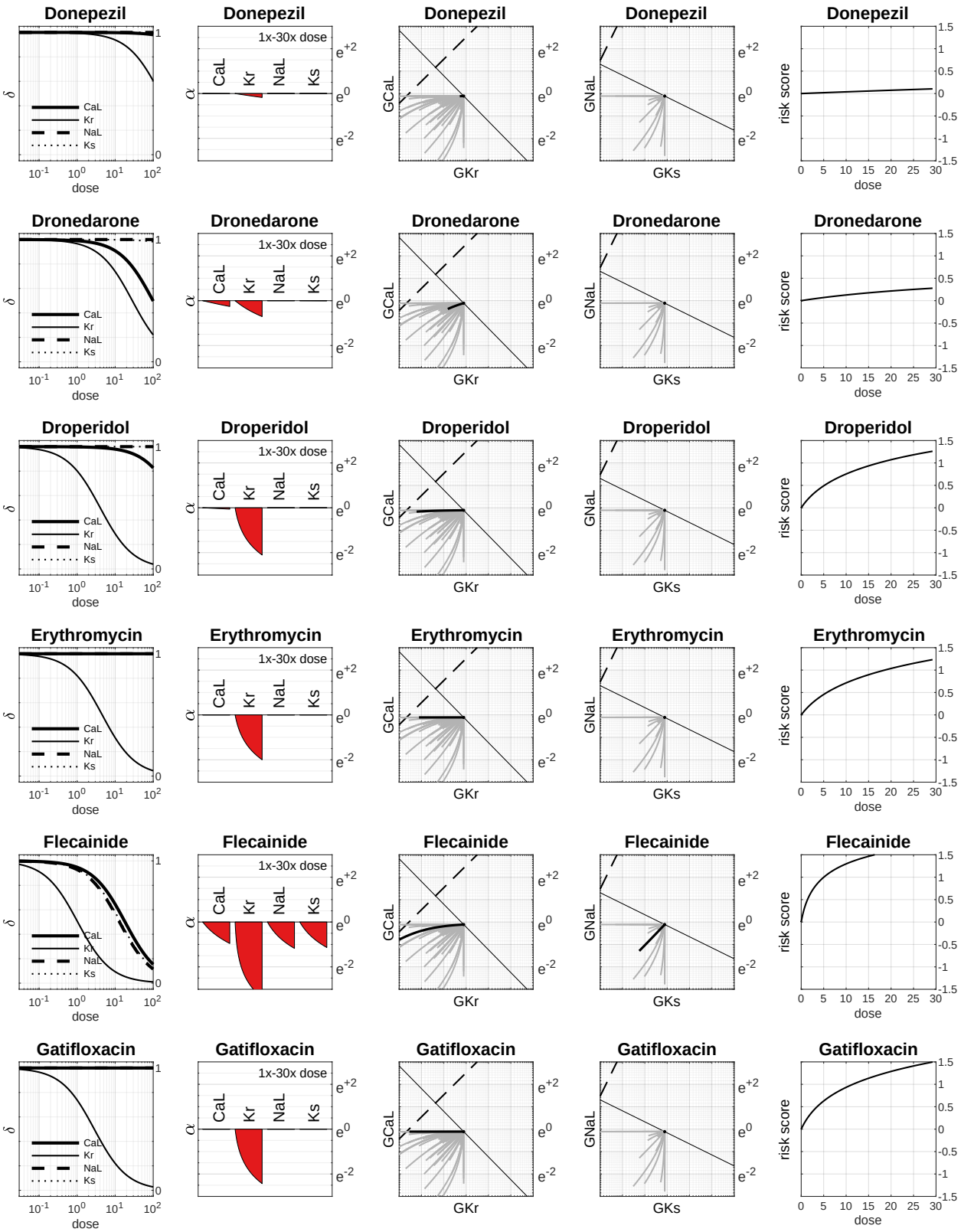
Donepezil
Dronedarone
Droperidol
Erythromycin
Flecainide
Gatifloxacin
δ
α
dose
risk score
CaL
Kr
NaL
Ks
1x-30x dose
GCaL
GKr
GNaL
GKs

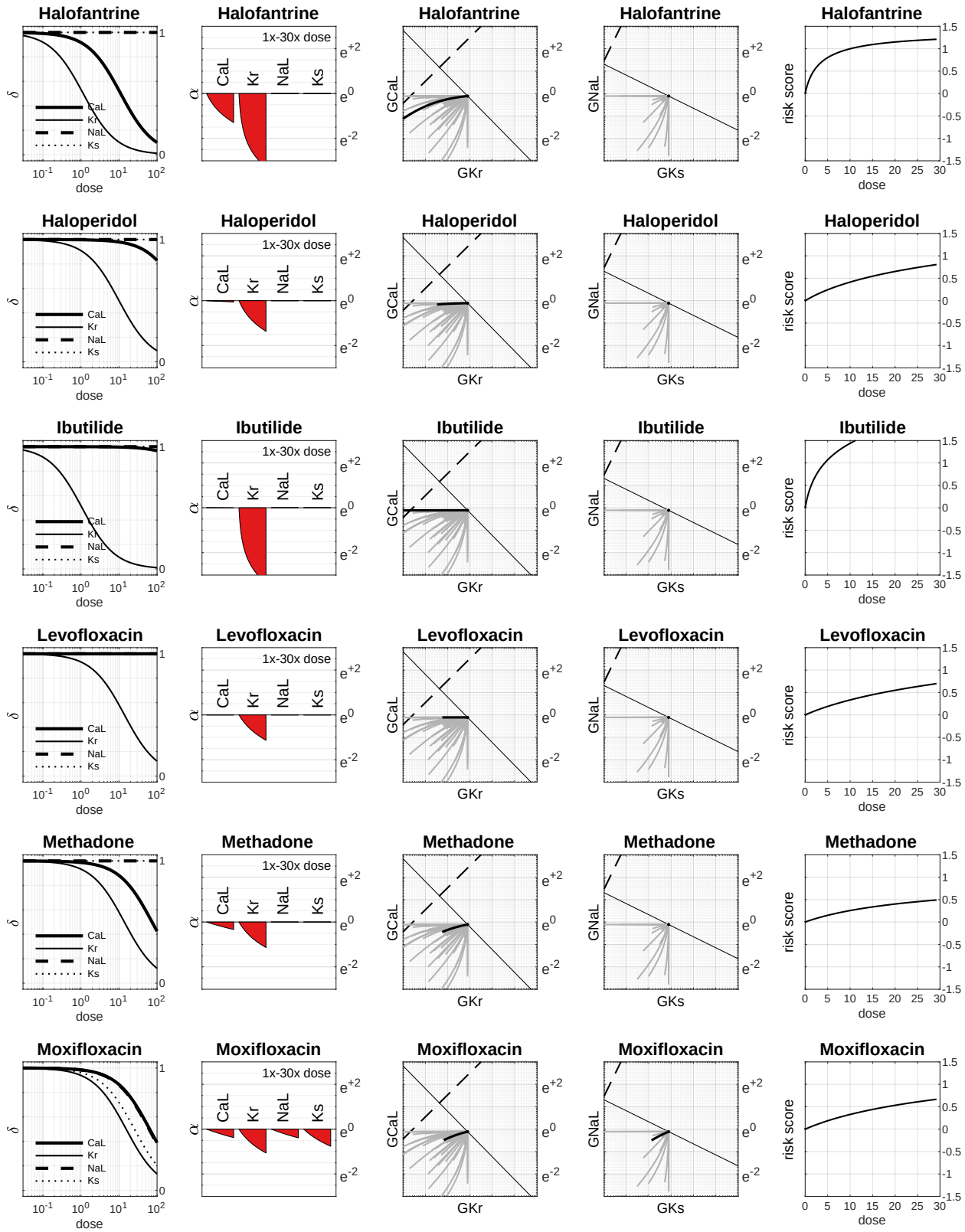
Halofantrine
Haloperidol
Ibutilide
Levofloxacin
Methadone
Moxifloxacin
δ
dose
CaL
Kr
NaL
Ks
1x-30x dose
α
GCaL
GKr
GNaL
GKs
risk score

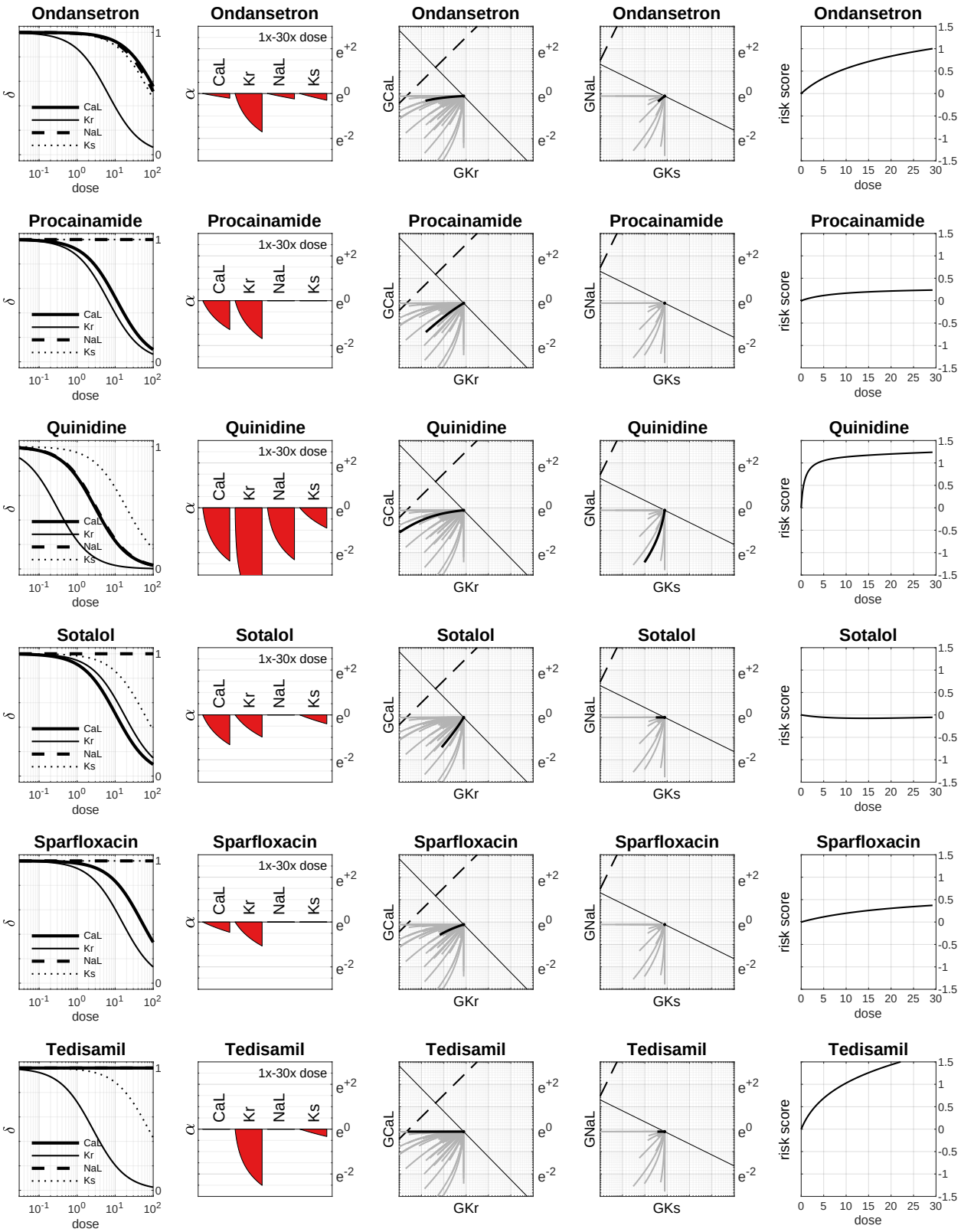
Ondansetron
Procainamide
Quinidine
Sotalol
Sparfloxacin
Tedisamil
δ
dose
CaL
Kr
NaL
Ks
1x-30x dose
α
GCaL
GKr
GNaL
GKs
risk score

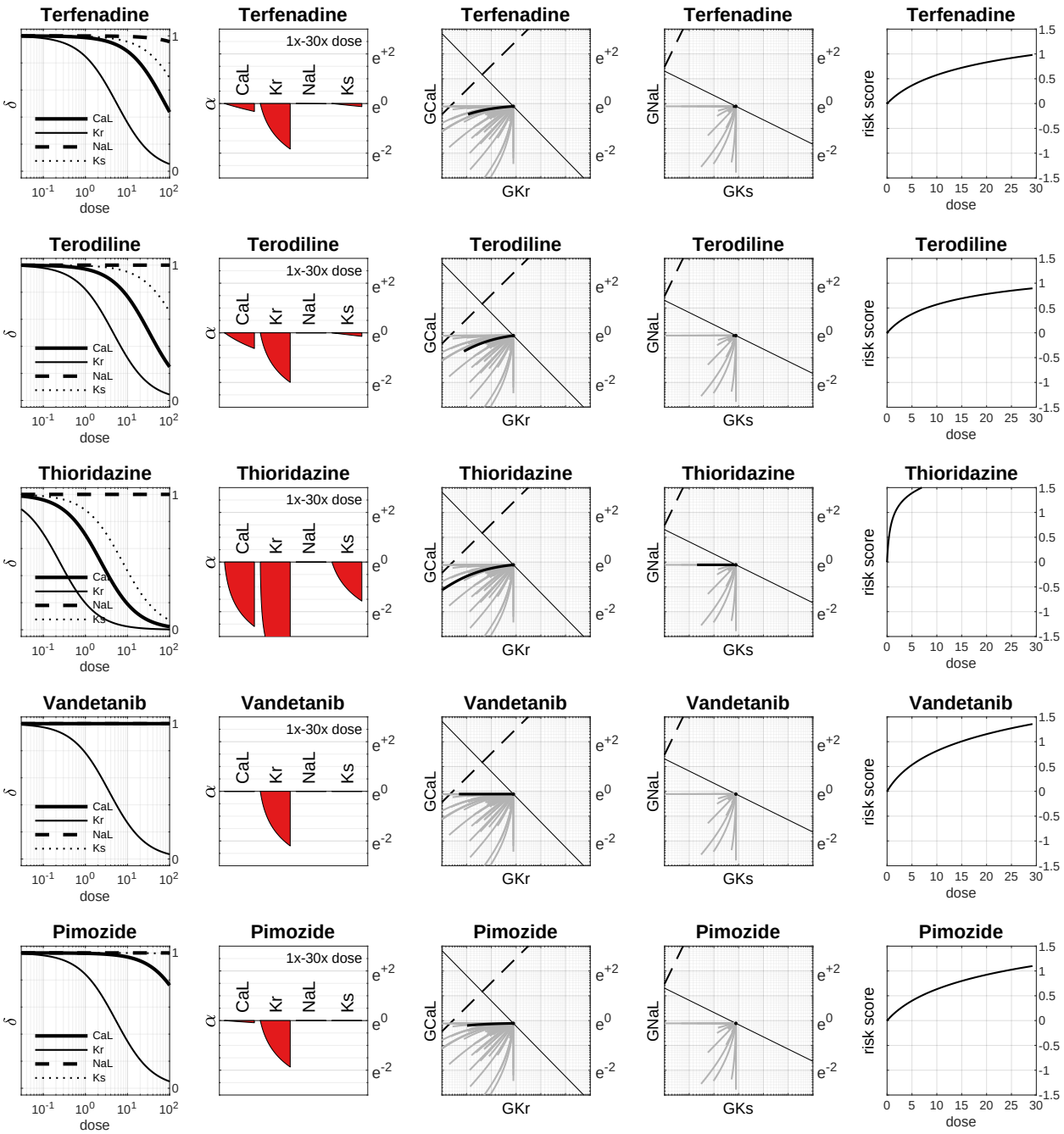
Terfenadine
Terodiline
Thioridazine
Vandetanib
Pimozide
δ
dose
CaL
Kr
NaL
Ks
1x-30x dose
α
GCaL
GKr
GNaL
GKs
risk score

Drugs with Class 2 Torsadogenic risk

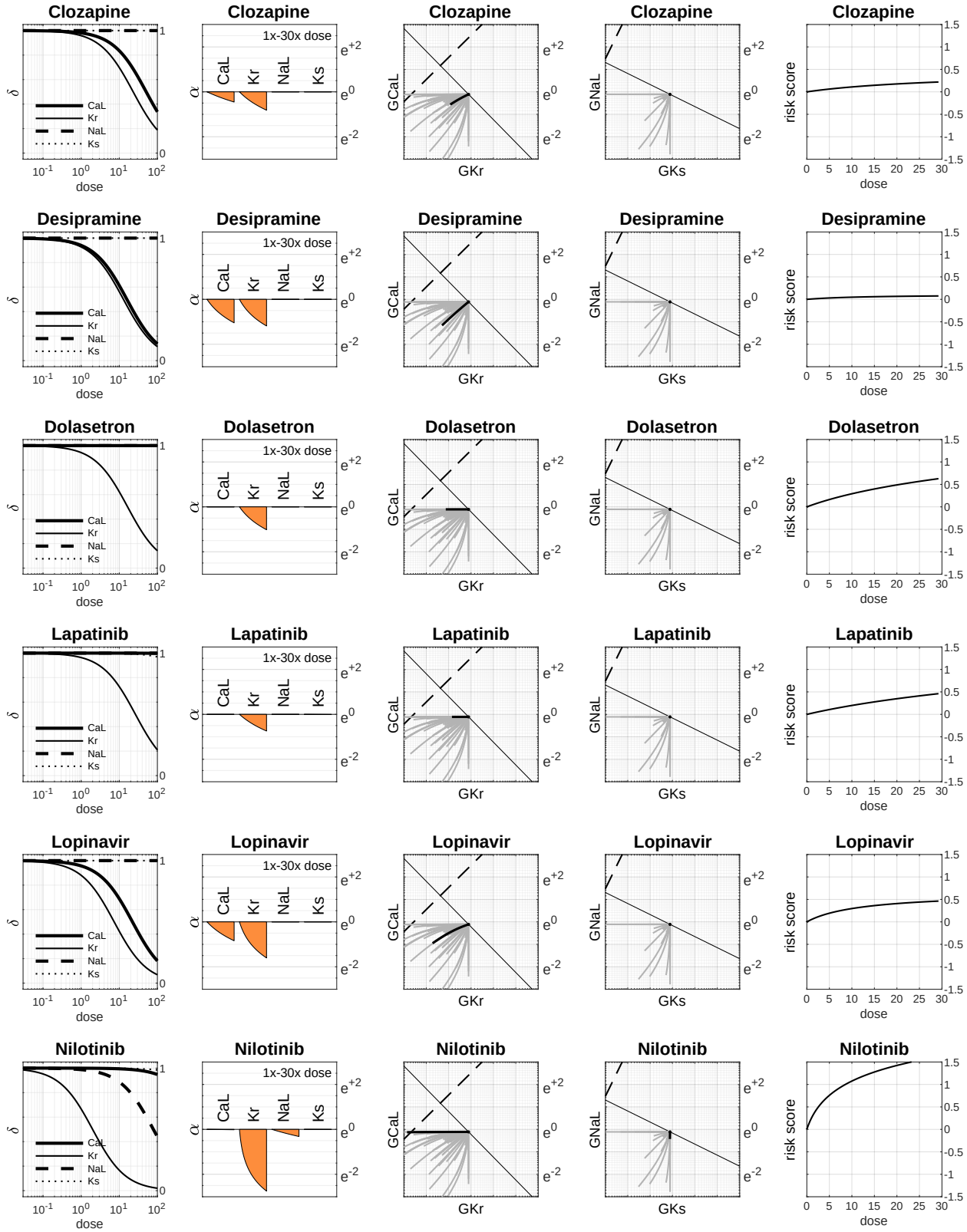

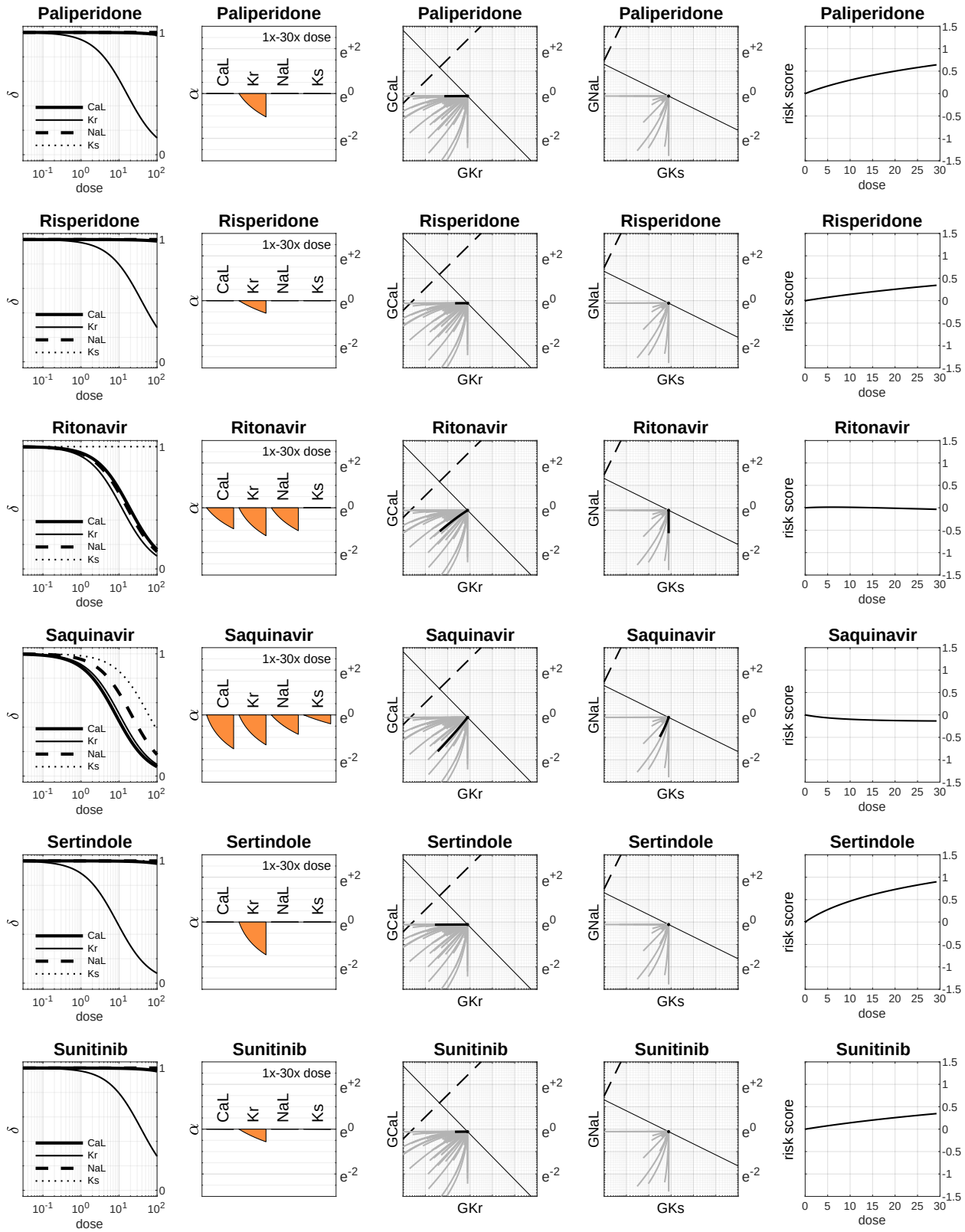
Paliperidone
Risperidone
Ritonavir
Saquinavir
Sertindole
Sunitinib
δ
dose
CaL
Kr
NaL
Ks
1x-30x dose
α
GCaL
GKr
GNaL
GKs
risk score

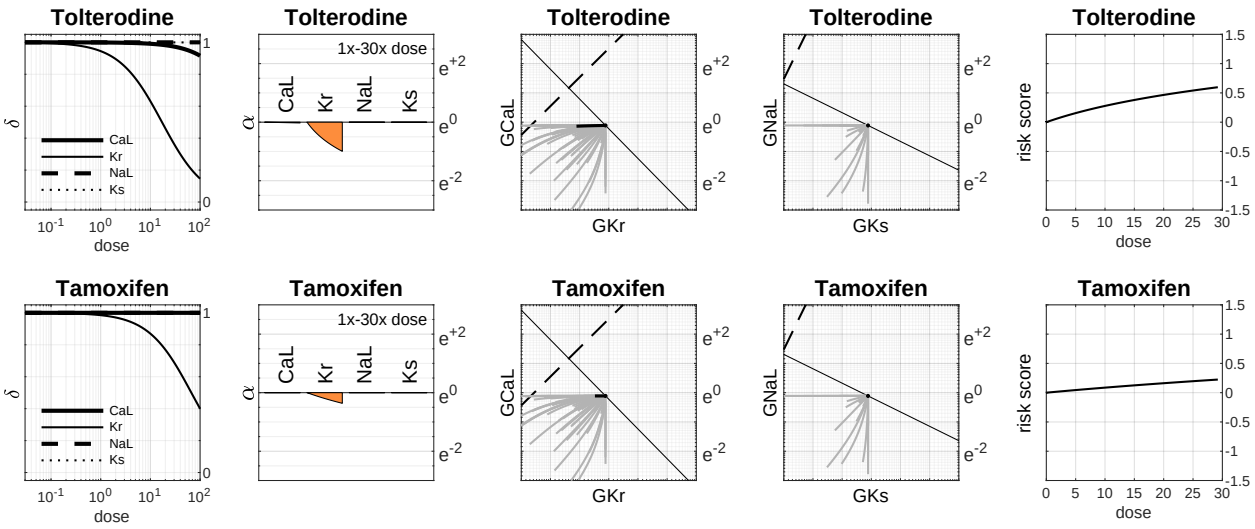

Drugs with Class 3 Torsadogenic risk

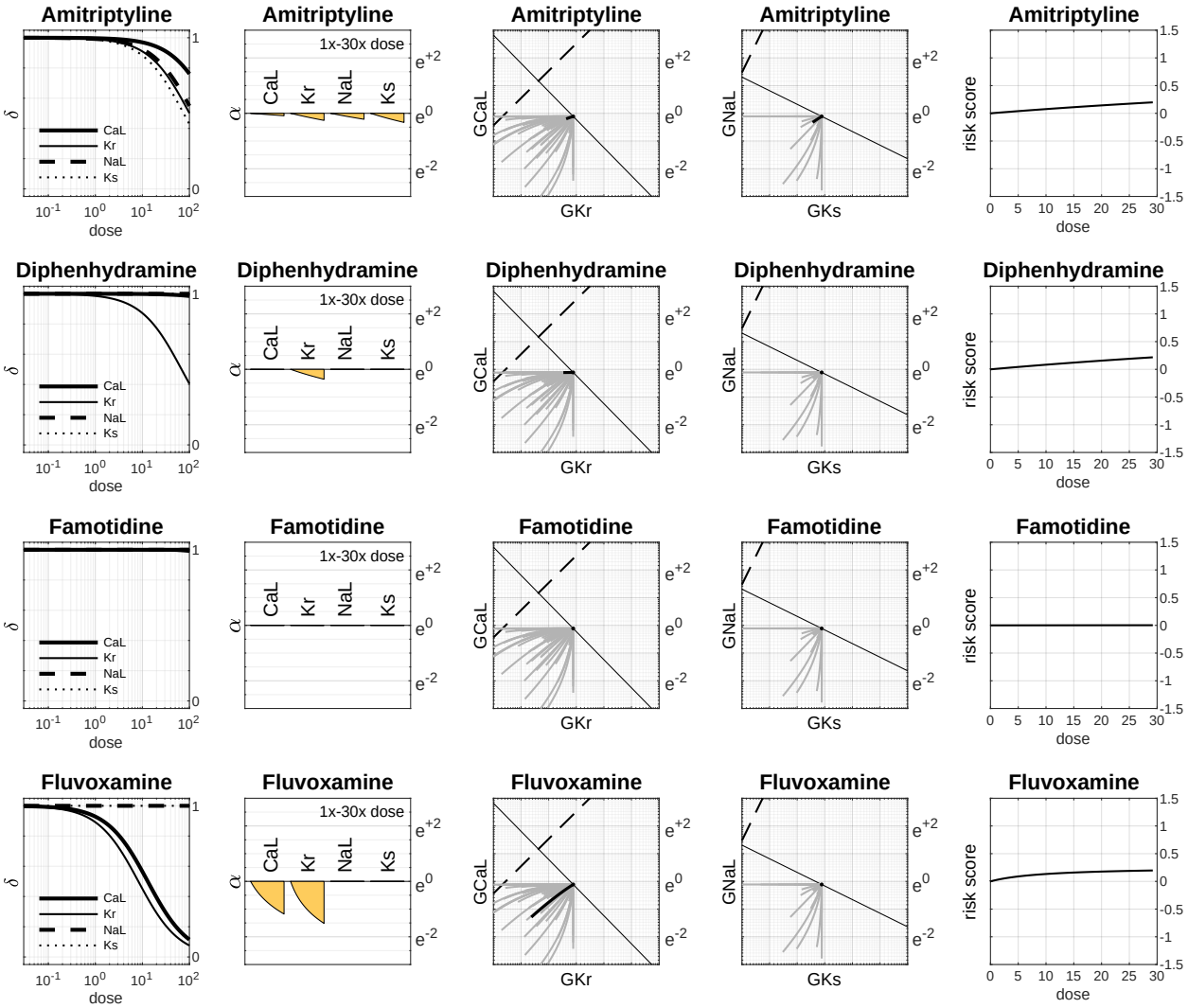

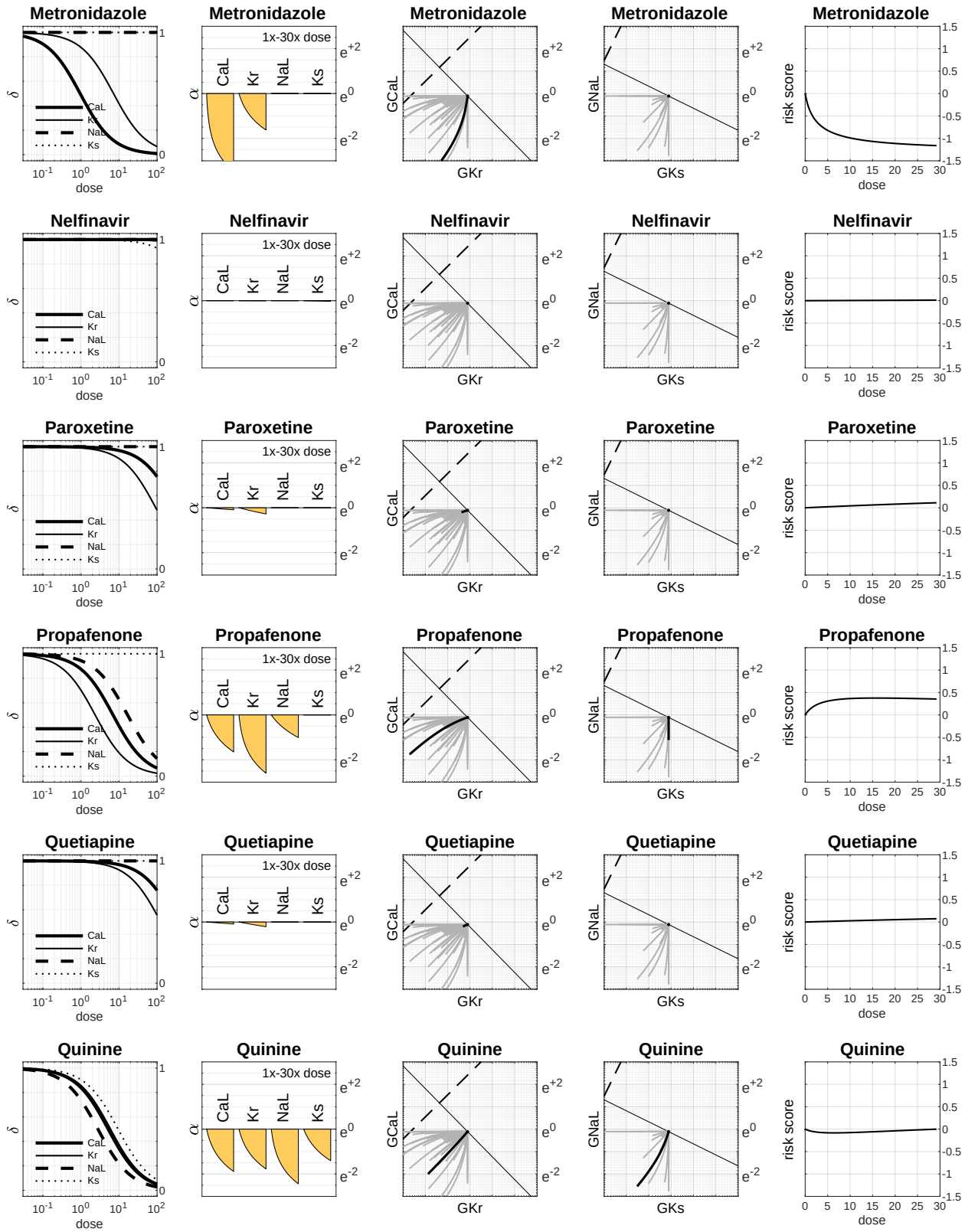
Metronidazole
Nelfinavir
Paroxetine
Propafenone
Quetiapine
Quinine
1x-30x dose
CaL
Kr
NaL
Ks
GCaL
GNaL
GKr
GKs
dose
risk score

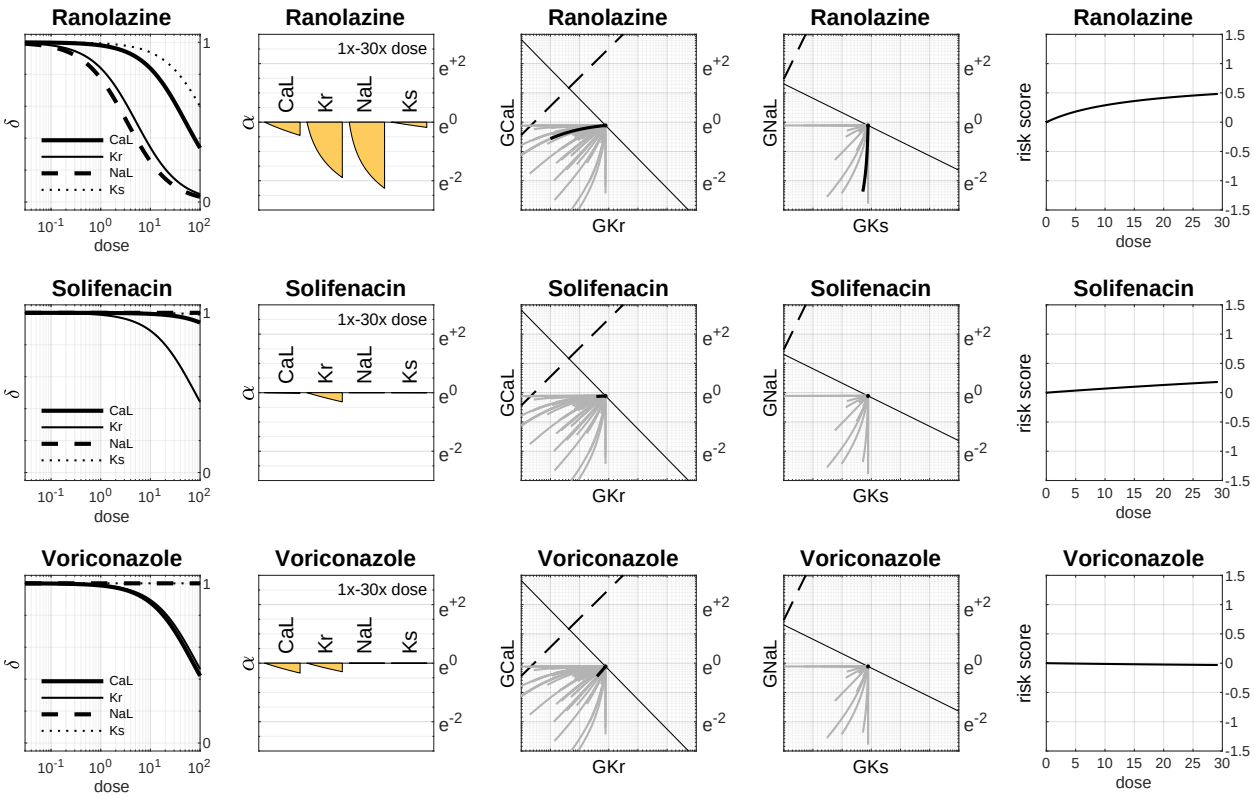

Drugs with Class 4 Torsadogenic risk

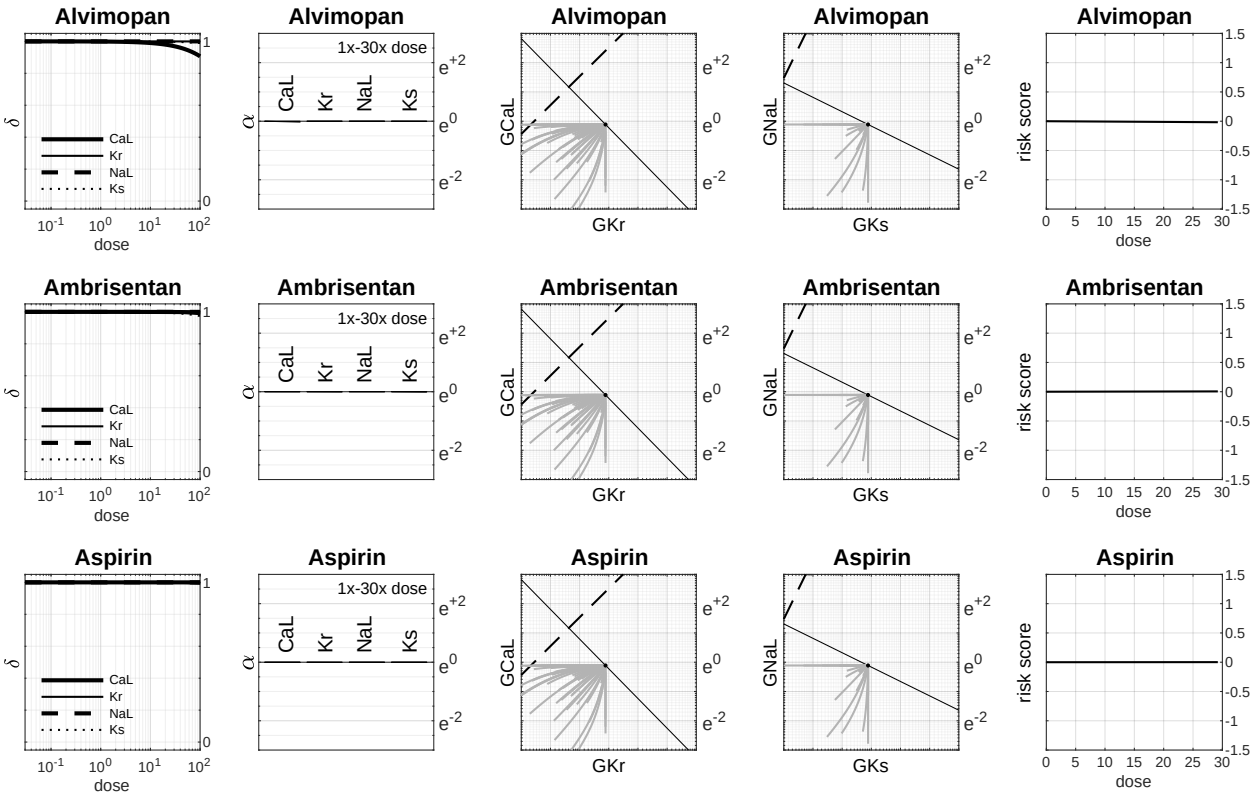

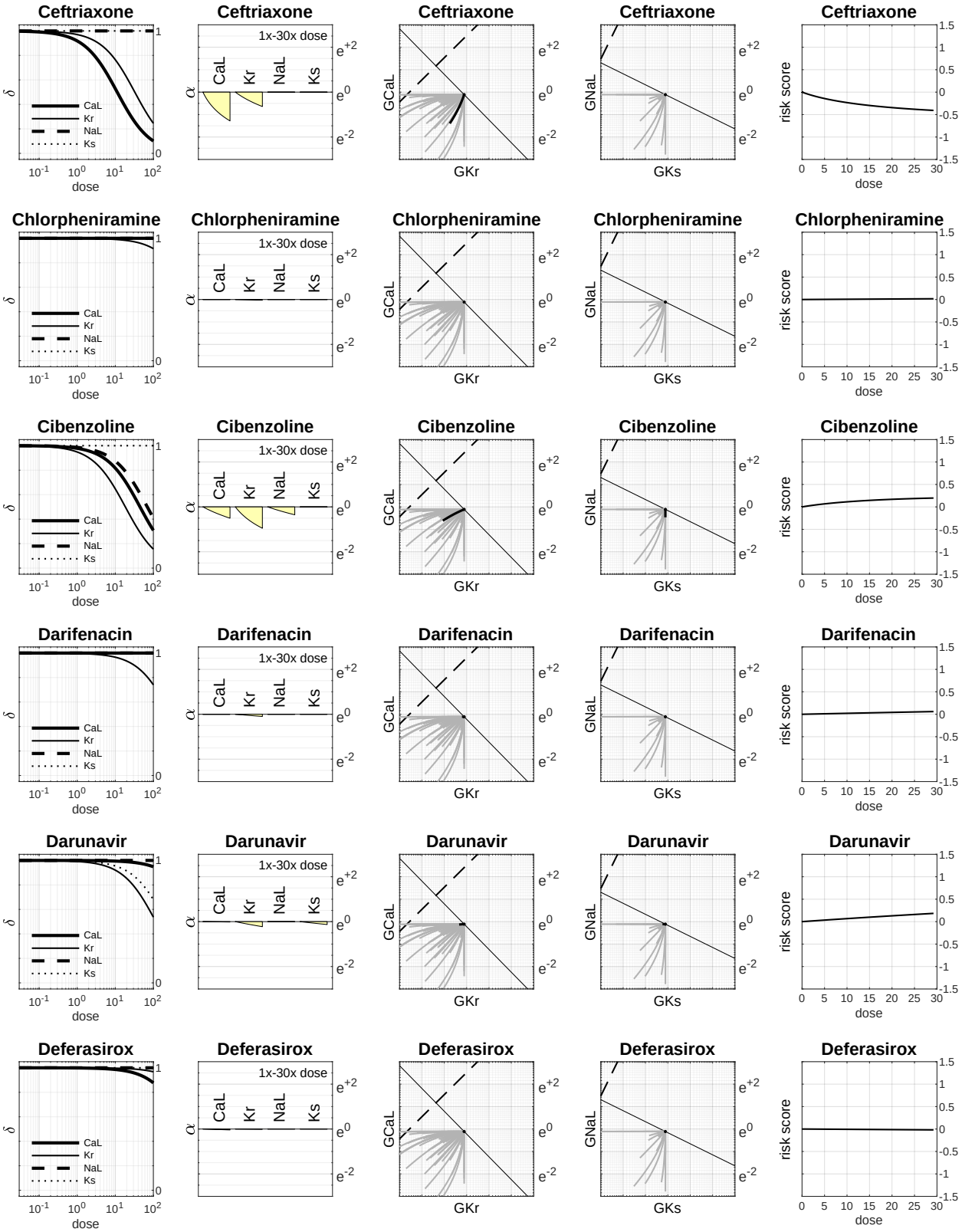
Ceftriaxone
Chlorpheniramine
Cibenzoline
Darifenacin
Darunavir
Deferasirox
δ
dose
CaL
Kr
NaL
Ks
1x-30x dose
α
GCaL
GKr
GNaL
GKs
risk score

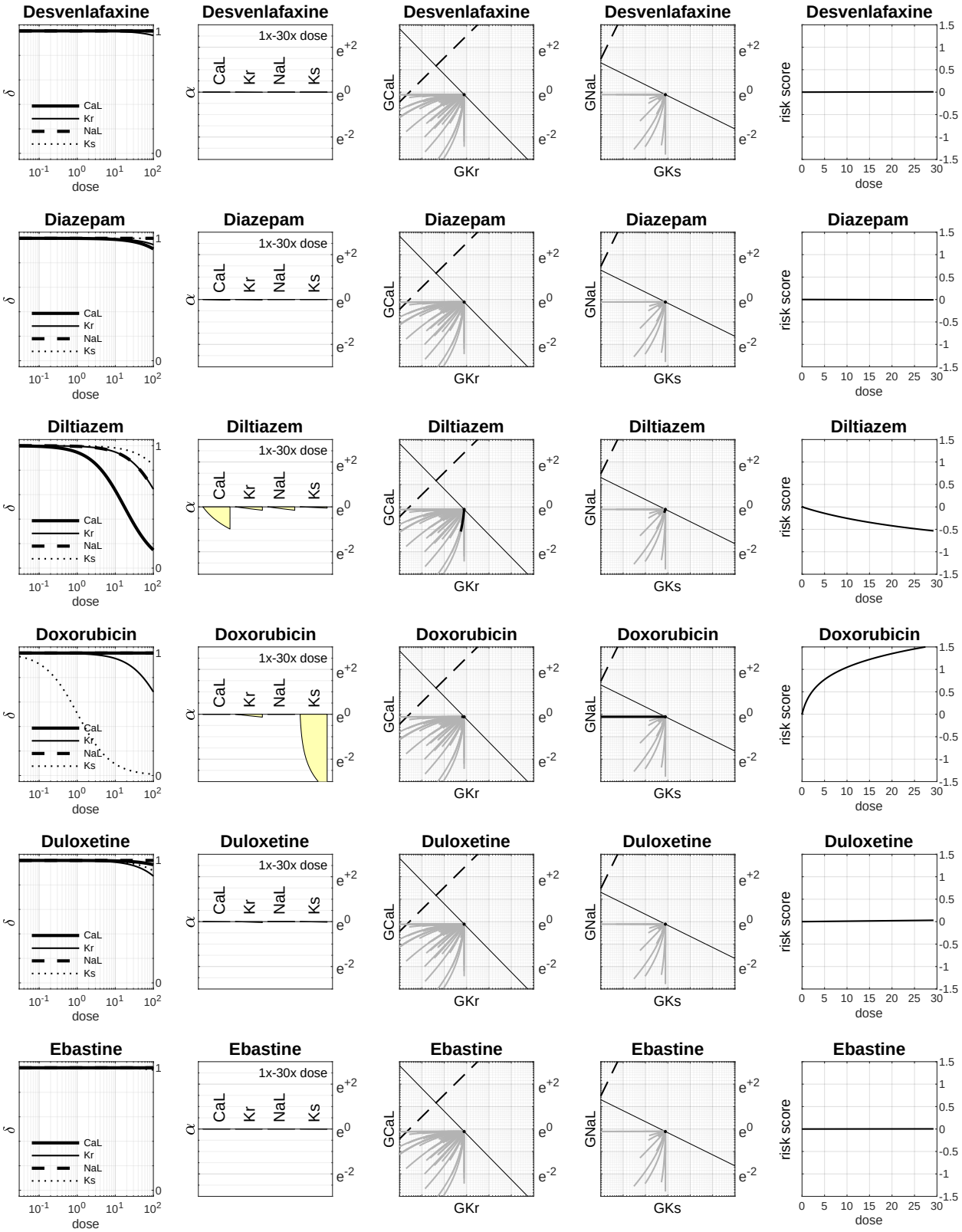
Desvenlafaxine
Diazepam
Diltiazem
Doxorubicin
Duloxetine
Ebastine
δ
dose
CaL
Kr
NaL
Ks
1x-30x dose
α
GCaL
GKr
GNaL
GKs
risk score

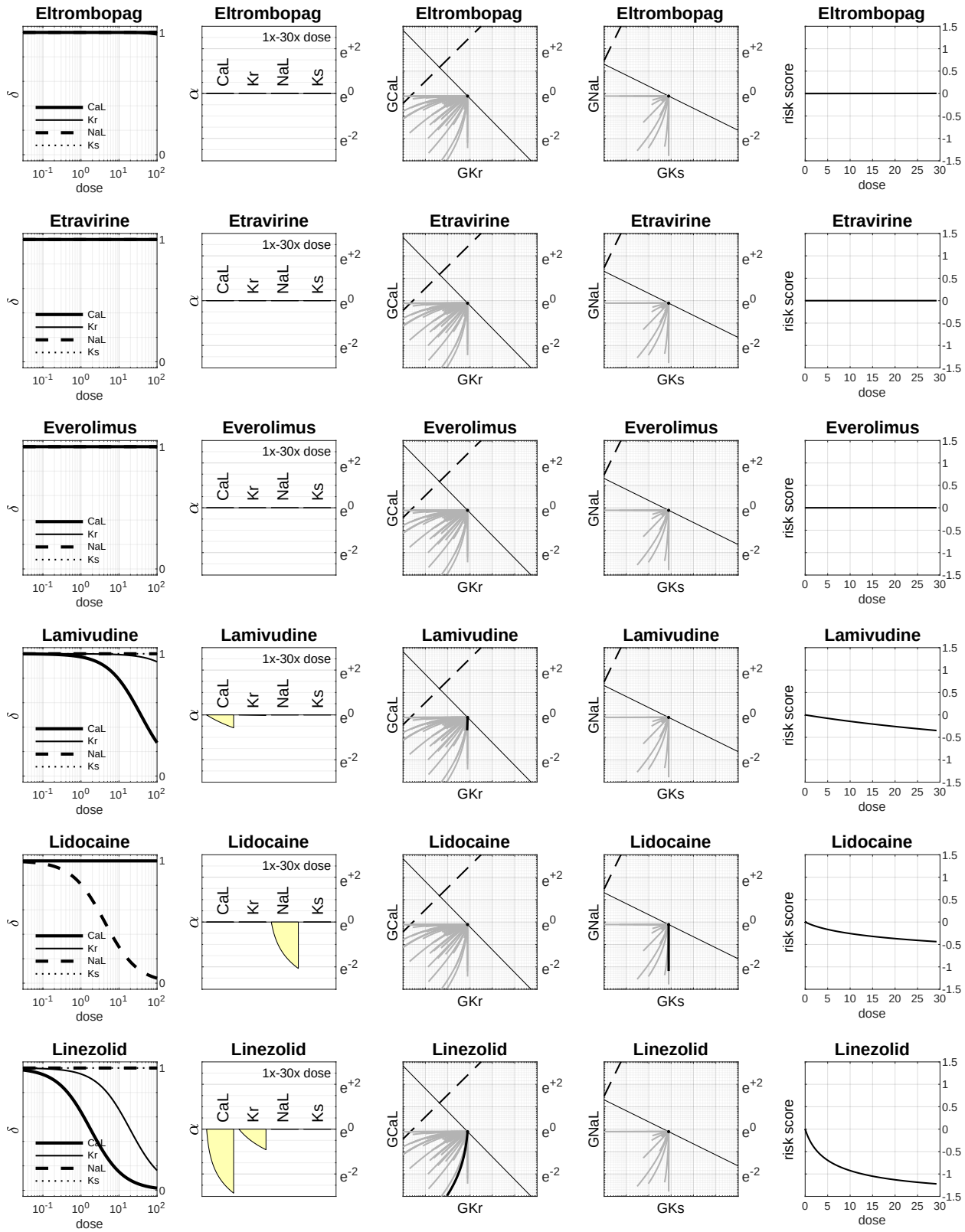
Eltrombopag
Etravirine
Everolimus
Lamivudine
Lidocaine
Linezolid
1x-30x dose
CaL
Kr
NaL
Ks
δ
α
dose
GCaL
GKr
GNaL
GKs
risk score

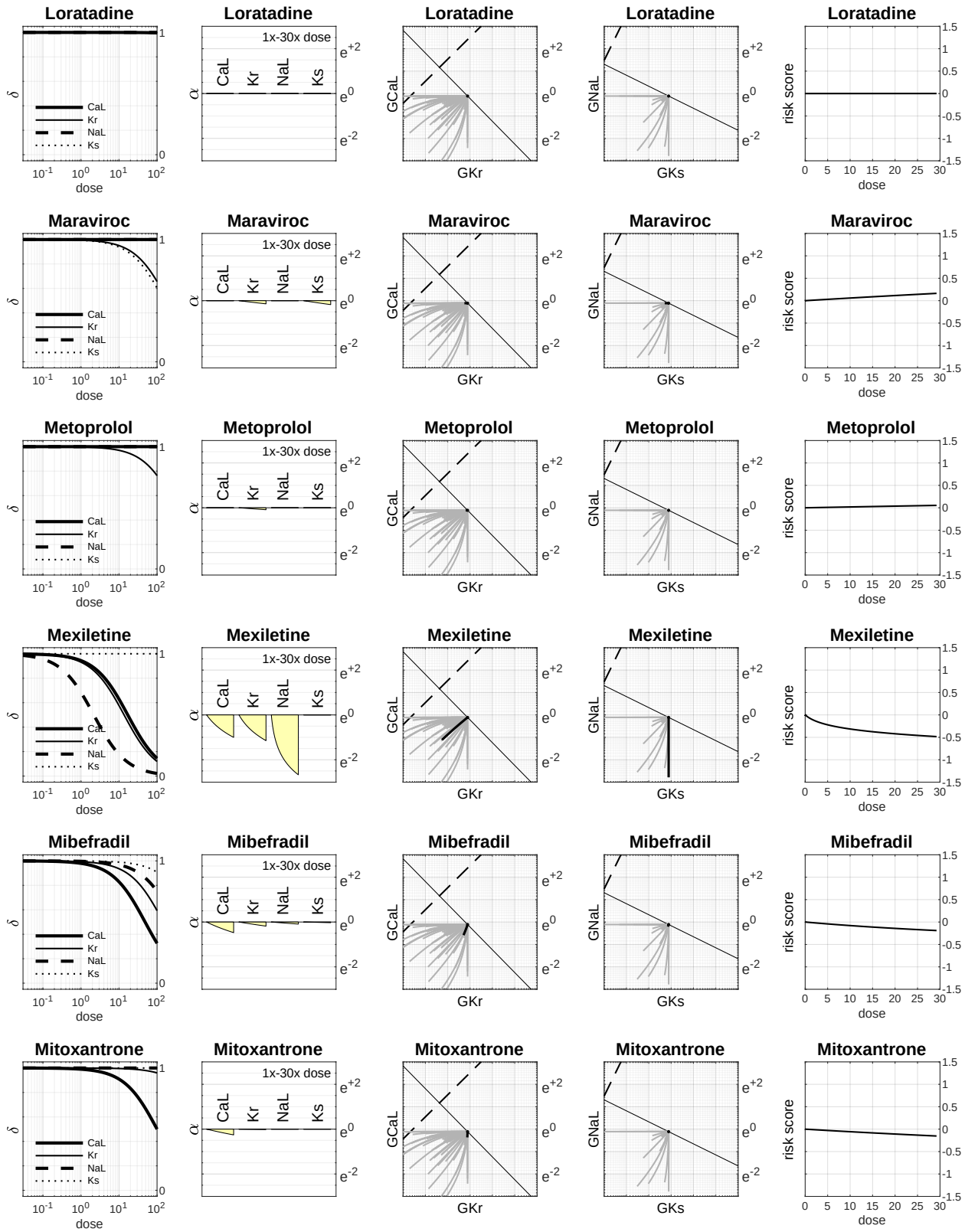
Loratadine
Maraviroc
Metoprolol
Mexiletine
Mibefradil
Mitoxantrone
δ
dose
CaL
Kr
NaL
Ks
1x-30x dose
α
GCaL
GKr
GNaL
GKs
risk score

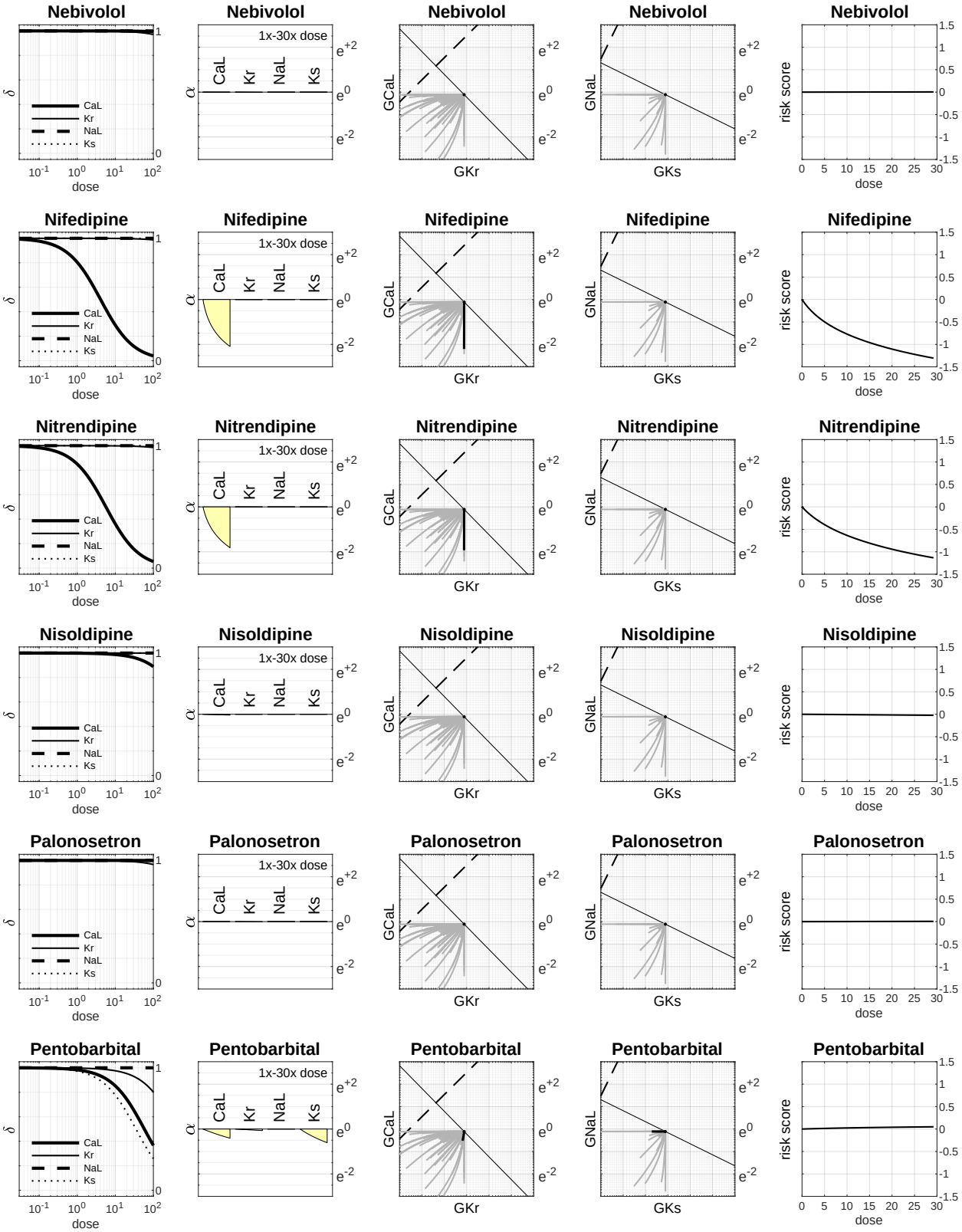
Nebivolol
Nifedipine
Nitrendipine
Nisoldipine
Palonosetron
Pentobarbital
δ
dose
CaL
Kr
NaL
Ks
1x-30x dose
α
GCaL
GKr
GNaL
GKs
risk score

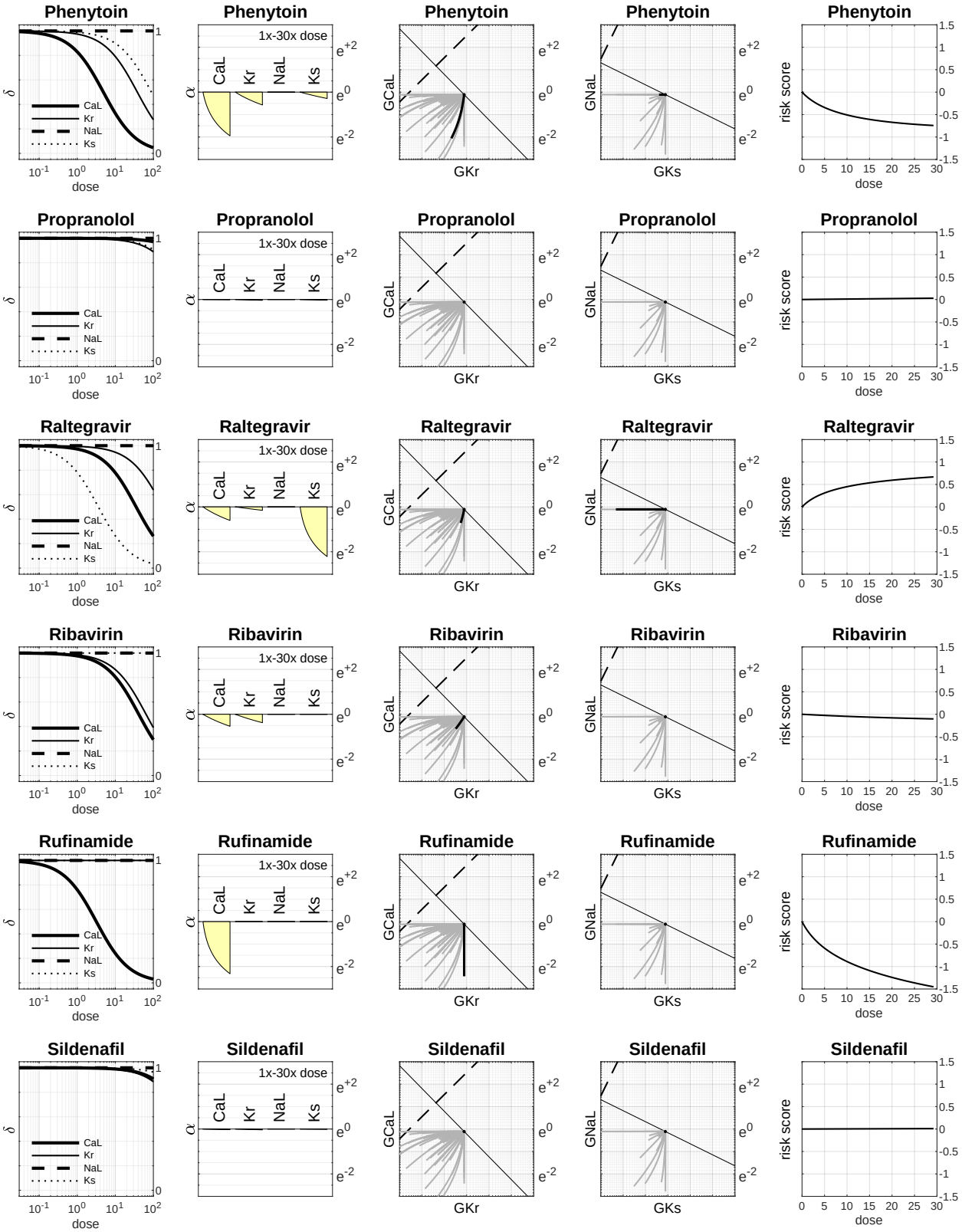
Phenytoin
Propranolol
Raltegravir
Ribavirin
Rufinamide
Sildenafil
δ
dose
CaL
Kr
NaL
Ks
1x-30x dose
α
GCaL
GKr
GNaL
GKs
risk score

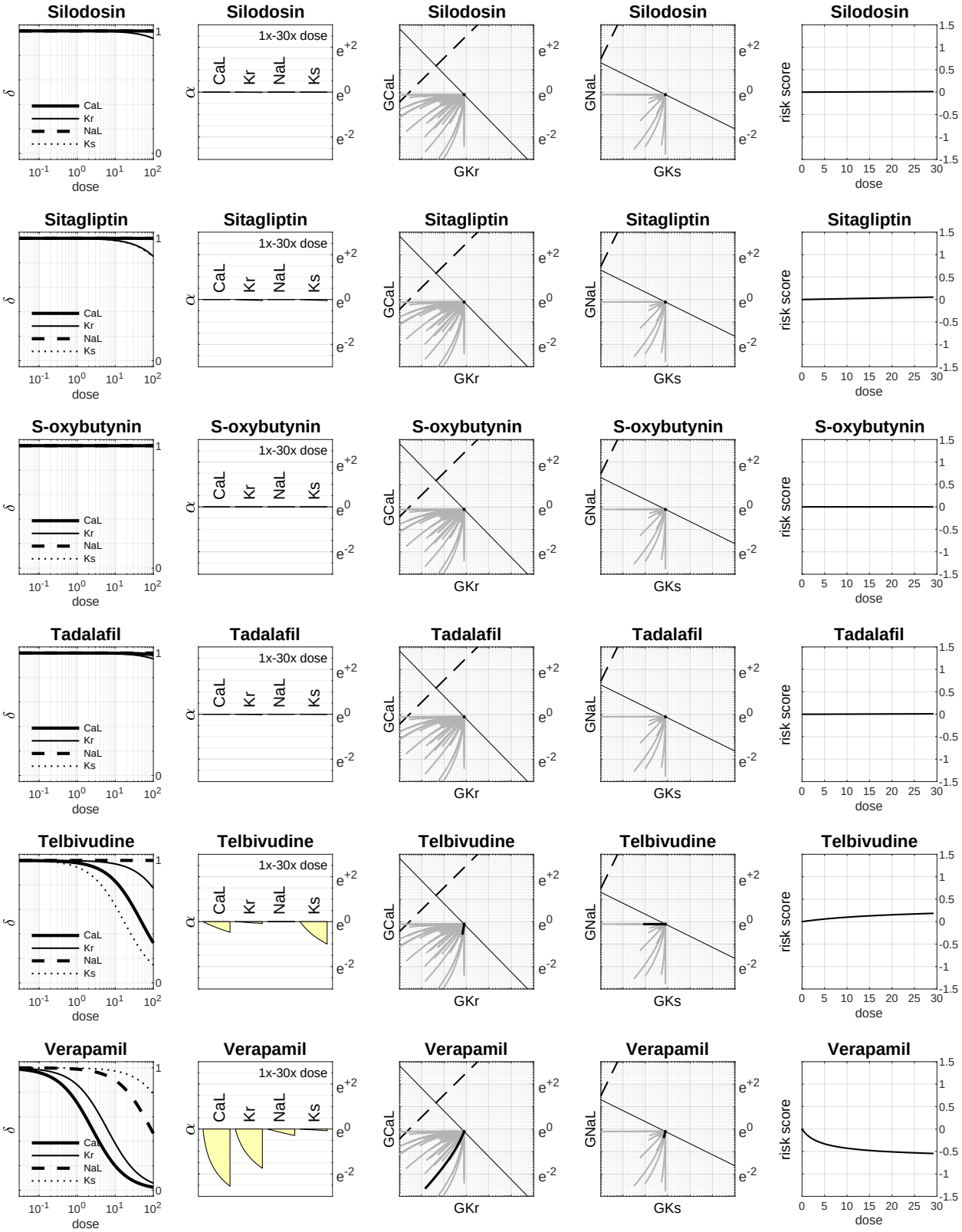
Silodosin
Sitagliptin
S-oxybutynin
Tadalafil
Telbivudine
Verapamil
δ
dose
CaL
Kr
NaL
Ks
1x-30x dose
α
GCaL
GKr
GNaL
GKs
risk score